Quantifying the drivers of surface ozone anomalies in the urban areas over the Qinghai-Tibet Plateau

Hao Yin [1, 2,★], Youwen Sun [1, 2,†,★], Justus Notholt [3], Mathias Palm [3], Chunxiang Ye [4], and Cheng Liu [2,5,6,7†]

[1] *Key Laboratory of Environmental Optics and Technology, Anhui Institute of Optics and Fine Mechanics, HFIPS, Chinese Academy of Sciences, Hefei 230031, China*

[2] *Department of Precision Machinery and Precision Instrumentation, University of Science and Technology of China, Hefei 230026, China*

[3] *University of Bremen, Institute of Environmental Physics, P. O. Box 330440, 28334 Bremen, Germany*

[4] *State Key Laboratory of Environmental Simulation and Pollution Control, College of Environmental Sciences and Engineering, Peking University, Beijing, China*

[5] *Anhui Province Key Laboratory of Polar Environment and Global Change, University of Science and Technology of China, Hefei 230026, China*

[6] *Center for Excellence in Regional Atmospheric Environment, Institute of Urban Environment, Chinese Academy of Sciences, Xiamen 361021, China*

[7] *Key Laboratory of Precision Scientific Instrumentation of Anhui Higher Education Institutes, University of Science and Technology of China, Hefei 230026, China*

[†]Corresponding authors.

[★]These authors contributed equally.

E-mail addresses: Youwen Sun (ywsun@aiofm.ac.cn) and Cheng Liu (chliu81@ustc.edu.cn)

Abstract

Improved knowledge of the chemistry and drivers of surface ozone over the Qinghai-Tibet Plateau (QTP) is significant for regulatory and control purposes in this high-altitude region in the Himalaya. In this study, we investigate the processes and drivers of surface ozone anomalies (defined as deviations of ozone levels relative to their seasonal means) between 2015 and 2020 in urban areas over the QTP. We separate quantitatively the contributions of anthropogenic emissions and meteorology to surface ozone anomalies by using the random forest (RF) machine learning model based meteorological normalization method. Diurnal and seasonal surface ozone anomalies over the QTP were mainly driven by meteorological conditions, such as temperature, planetary boundary layer height, surface incoming shortwave flux, downward transport velocity, and inter-annual anomalies were mainly driven by anthropogenic emission. Depending on region and measurement hour, diurnal surface ozone anomalies varied over -27.82 μg/m^3 to 37.11 μg/m^3, where meteorological and anthropogenic contributions varied over -33.88 μg/m^3 to 35.86 μg/m^3 and -4.32 μg/m^3 to 4.05 μg/m^3, respectively. Exceptional meteorology driven 97% of surface ozone nonattainment events from 2015 to 2020 in the urban areas over the QTP. Monthly averaged surface ozone anomalies from 2015 to 2020 varied with much smaller amplitudes than their diurnal anomalies, where meteorological and anthropogenic contributions varied over 7.63 μg/m^3 to 55.61 μg/m^3 and 3.67 μg/m^3 to 35.28 μg/m^3, respectively. The inter-annual trends of surface ozone in Ngari, Lhasa, Naqu, Qamdo, Diqing, Haixi and Guoluo can be attributed to anthropogenic emissions by 95.77%, 96.30%, 97.83%, 82.30%, 99.26%, and 87.85%, and meteorology by 4.23%, 3.70%, 2.17%, 3.19%, 0.74%, and 12.15%, respectively. The inter-annual trends of surface ozone in other cities

1   were fully driven by anthropogenic emission, where the increasing inter-annual trends would have
2   larger values if not for the favorable meteorological conditions. This study can not only improve
3   our knowledge with respect to spatiotemporal variability of surface ozone but also provides valuable
4   implication for ozone mitigation over the QTP.

1. Introduction

6   The Qinghai-Tibet Plateau (QTP) (27-45° N, 70-105° E), with an average altitude of 4000m
7   above sea level (a.s.l), is the highest plateau in the world. It is known as the "Roof of the World"
8   and the "Third Pole" (Qiu, 2008;Yang et al., 2013;Yin et al., 2017). The QTP has an area of
9   approximately 2.5×10^6 km^2 and accounts for about one quarter of China's territory (Duo et al., 2018).
10   The QTP is the source region of five major rivers in Asia, i.e., the Indus, Ganges, Brahmaputra,
11   Yangtze, and Yellow rivers, which provide water resource to more than 1.4 billion people
12   (Immerzeel et al., 2010). The QTP has been verified to be a critical region for regulating Asian
13   monsoon climate and hydrological cycle, and it is thus an important ecological barrier of the whole
14   Asia (Loewen et al., 2007;Yanai et al., 1992). The QTP has long been regarded as a pristine region
15   due to its low population and industrial levels (Zhu et al., 2013). Due to its unique features of
16   landform, ecosystem and monsoon circulation pattern, the QTP has been regarded as a sensitive
17   region to anthropogenic impact, and is referred to as an important indicator of regional and global
18   climate change (Qiu, 2008). The exogenous and local atmospheric pollutants are potential to
19   accelerate the melting of glaciers, damage air quality, water sources, and grasslands, and threaten
20   climate on regional and global scales (Yin et al., 2017;Yin et al., 2019c;Sun et al., 2021d;Pu et al.,
21   2007;Kang et al., 2016). Therefore, improved knowledge of the evolutions and drivers of
22   atmospheric pollutants in the QTP is of great importance for understanding local ecological situation
23   and formulating regulatory policies.

24   Surface ozone (O$_3$) is a major air pollutant that threatens human health and vegetation growth
25   (Jerrett et al., 2009;Yin et al., 2021b). Surface ozone over the QTP is generated either from its local
26   anthropogenic and natural precursors such as nitrogen oxides (NO$_x$), volatile organic compounds
27   (VOCs), and carbon monoxide (CO) via a chain of photochemical reactions or transported from
28   long-distance regions by downwelling from the stratosphere. Surface ozone level is sensitive to local
29   emissions, meteorological conditions and transport. Meteorological conditions affect surface ozone
30   level indirectly through changes in natural emissions of its precursors or directly via changes in wet
31   and dry removal, dilution, chemical reaction rates, and transport flux. Emissions of air pollutants
32   affect surface ozone level by perturbing the abundances of hydroperoxyl (HO$_2$) and alkylperoxyl
33   (RO$_2$) radicals which are the key atmospheric constituents in formation of ozone. Some previous
34   studies have presented the variability and analyzed qualitatively the drivers of surface ozone over
35   the QTP at a specific site or region (Xu et al., 2016;Yin et al., 2019b;Yin et al., 2017;Zhu et al.,
36   2004). However, none of these studies have quantitatively separated the contributions of
37   anthropogenic emission and meteorology. Separation of anthropogenic and meteorological drivers
38   is very important since it conveys us exactly which processes drive the observed ozone anomaly
39   and therefore right conclusions can be made on whether an emission mitigation policy is effective.

40   Chemical transport models (CTMs) are widely used to evaluate the influences of meteorology
41   and anthropogenic emission on atmospheric pollution levels (Hou et al., 2022;Sun et al., 2021a;Yin
42   et al., 2020;Yin et al., 2019a). However, there are significant uncertainties in the emission
43   inventories and in the models themselves, and shutting down an emission inventory in CTMs may

cause large nonlinear effect, which inevitably influences the accuracy, performance and efficient of CTMs (Vu et al., 2019;Zhang et al., 2020). Mathematical and statistical models such as the multiple linear regression (MLR) model and general additive models (GAMs) have also been used in many studies to quantify the influence of meteorological factors (Li et al., 2019;Li et al., 2020a;Yin et al., 2021a;Yin et al., 2022;Zhai et al., 2019).

Machine learning (ML) is a well-known field that has been developing rapidly in recent years. Machine learning is a fusion of statistics, data science, and computing which experiences use across a very wide range of applications (Grange et al., 2018). Unlike most ML models such as artificial neural networks which are hard to understand the working mechanisms, the random forest (RF) model is not a "black-box" method, its prediction process can be explained, investigated, and understood (Gardner and Dorling, 2001;Grange et al., 2018;Grange and Carslaw, 2019;Shi et al., 2021). Recently, RF model based meteorological normalization technique has been proposed and used to decouple the meteorological influence on atmospheric pollution. For example, Vu et al. (Vu et al., 2019) have used this technique to demonstrate that the clean air action plan implemented in 2013 was highly effective in reducing the anthropogenic emissions and improving air quality in Beijing. Shi et al. (Shi et al., 2021) have used this technique to quantitatively evaluate changes in ambient NO_2, ozone, and $PM_{2.5}$ concentrations arising from these emission changes in 11 cities globally during the COVID-19 lockdowns.

In this study, we investigate the evolutions, implications, and drivers of surface ozone anomalies (defined as deviations of ozone levels relative to their seasonal means) from 2015 to 2020 in the urban areas over the QTP. Compared with previous studies that focus on surface ozone over the QTP, this study involves in larger area and longer time span. Most importantly, this study separates quantitatively the contributions of anthropogenic emission and meteorology to surface ozone anomalies by using the RF model based meteorological normalization method. This study can not only improve our knowledge with respect to spatiotemporal variability of surface ozone but also provides valuable implication for ozone mitigation over the QTP. We introduce detailed descriptions of surface ozone and meteorological field dataset in section 2. The method for separating contributions of meteorology and anthropogenic emission is presented in section 3. Section 4 analyzes spatiotemporal variabilities of surface ozone from 2015 to 2020 in each city over the QTP. The performance of the RF model used for surface ozone prediction over the QTP is evaluated in Section 5. We discuss the implications and the drivers of surface ozone anomalies from 2015 to 2020 in each city over the QTP in section 6. We conclude this study in section 7.

2. Data sources

2.1 Surface ozone data

The QTP covers an area of 2.5 million square meter and has a population of around 3 million, with most of them living in several cities. During the in depth study of the atmospheric chemistry over the Tibetan Plateau, @Tibet field campaign, ozone photochemistry and its roles in ozone budget are of great interests in both background atmosphere and in QTP urban areas. The former represents the influence of anthropogenic emission and cross boundary transport on the nature cycle of ozone in pristine atmosphere. The latter represents not only the upper limit of ozone photochemistry contribution to its budget, also a demanding knowledge for the sake of ozone pollution management. As illustrated in Figure 1, the QTP (Latitude range: 26°00' ~ 39°47', Longitude range: 73°19' ~ 104°47') covers the Kunlun Mountain, the A-erh-chin Mountain and the

Qilian Mountain in the north, the Pamir Plateau and the Karakorum Mountains in the west, the Himalayas in the south, and the Qinling Mountains and the Loess Plateau in the east. These 12 cities are the most populated areas over the QTP. All these cities except Aba and Diqing are located in Tibet or Qinghai provinces. Aba and Diqing are in Sichuan and Yunnan provinces, respectively. The area of these cities ranges from 7.7 to 430 thousand km^2, the altitude ranges from 2.3 to 4.8 km a.s.l., and the population ranges from 0.12 to 2.47 million. The residents within the 12 cities are about 3.85 million account for about 51% of population over the QTP.

Hourly surface ozone data in the urban areas over the QTP are available from the China National Environmental Monitoring Center (CNMEC) network (http://www.cnemc.cn/en/, last access: November 26, 2021). The CNMEC network based ozone measurements have been widely used in many studies for evaluation of regional atmospheric pollution and transport over China (Lu et al., 2021;Lu et al., 2019a;Lu et al., 2020;Sun et al., 2021c;Sun et al., 2021d;Yin et al., 2021a;Yin et al., 2021b;Yin et al., 2022).The CNEMC network has deployed 33 measurement sites in 12 cities over the QTP (Table 1). The number of measurement sites in each city varies from 1 to 6. All surface ozone time series at each measurement site are provided by active differential absorption ultraviolet (UV) analyzers. For all the 33 measurement sites, hourly surface ozone data are available since 2015. We first removed unreliable measurements at all measurement sites in each city by using the filter criteria following our previous studies (Lu et al., 2018;Lu et al., 2020;Sun et al., 2021b;Sun et al., 2021d;Yin et al., 2021a;Yin et al., 2021b), then averaged all measurements in each city to generate a city representative dataset. All investigations in this study are performed on such city representative basis.

The filter criteria can be summarized as follows. Hourly observed data points were first transformed into Z scores via equation (1) and the observed data were then removed if the corresponding Z_i value met one of the following conditions: (1) Z_i is larger or smaller than the previous one (Z_{i-1}) by 9 ($|Z_i - Z_{i-1}| > 9$), (2) The absolute value of Z_i is greater than 4 ($|Z_i| > 4$), or (3) the ratio of the Z value to the third-order center moving average is greater than 2 ($\frac{3Z_i}{Z_{i-1}+Z_i+Z_{i+1}} > 2$).

$$Z_k = \frac{x_k - u_k}{\sigma_k} \tag{1}$$

where u_k and σ_k are the average and 1σ standard deviation (STD) of x_k, and Z_k is the pre-processed value for parameter x_k.

2.2 Meteorological data

Meteorological fields used in this study are from the Modern-Era Retrospective analysis for Research and Applications Version 2 (MERRA-2) dataset (Gelaro et al., 2017). The MERRA-2 dataset is produced by the NASA Global Modeling and Assimilation Office and it can provide time series of many meteorological variables with a spatial resolution of 0.5° × 0.625° (The NASA Global Modeling and Assimilation Office (GMAO)). The boundary layer height and surface meteorological variables are available per hour and other meteorological variables are available every 3 hours. It has been verified that the MERRA-2 meteorological fields over the QTP are in good agreement with the observations (Wang and Zeng, 2012;Xie et al., 2017). This MERRA-2 dataset has been extensively used in evaluations of regional atmospheric pollution formation and transport over China (Carvalho, 2019;Kishore Kumar et al., 2015;Song et al., 2018;Zhou et al., 2017;Li et al.,

2019;Li et al., 2020a;Yin et al., 2022;Zhai et al., 2019).

3. Methodology

3.1 Quantifying seasonality and inter-annual variability

We quantify the seasonality and inter-annual variability of surface ozone from 2015 to 2020 in each city over the QTP by using a bootstrap resampling method. The principle of such bootstrap resampling method was described in detail in Gardiner et al. (Gardiner et al., 2008). Many studies have verified the robustness of Gardiner's methodology in modeling the seasonality and inter-annual variabilities of a suite of atmospheric species (Sun et al., 2020;Sun et al., 2021a;Sun et al., 2021b;Sun et al., 2021d;Sun et al., 2018). In this study, we used a second Fourier series plus a linear function to fit surface ozone monthly mean time series from 2015 to 2020 over the QTP. The usage of measurements on monthly basis can improve the fitting correlation and lower the regression residual. As a result, the relationship between the measured and bootstrap resampled surface ozone monthly mean time series can be expressed as,

$$V(t, \mathbf{b}) = b_0 + b_1 t + b_2 \cos\left(\frac{2\pi t}{12}\right) + b_3 \sin\left(\frac{2\pi t}{12}\right) + b_4 \cos\left(\frac{4\pi t}{12}\right) + b_5 \sin\left(\frac{4\pi t}{12}\right) \qquad (2)$$

$$F(t, a, \mathbf{b}) = V(t, \mathbf{b}) + \varepsilon(t) \qquad (3)$$

where $F(t, a, \mathbf{b})$ and $V(t, \mathbf{b})$ represent the measured and fitted surface ozone time series, respectively. The parameters $b_0 - b_5$ contained in the vector $\mathbf{b}$ are coefficients obtained from the bootstrap resampling regression with $V(t, \mathbf{b})$. The b_0 is the intercept, and the b_1 is the annual growth rate, and b_1/b_0 is the inter-annual trend discussed below. The parameters $b_2 - b_5$ describe the seasonality, *t* is the measurement time in month elapsed since January 2015, and $\varepsilon(t)$ represents the residual between the measurements and the fitting results. The autocorrelation in the residual can increase the uncertainty in calculation of inter-annual trend. In this study, we have followed the procedure of Santer et al. (Santer et al., 2008) and included the uncertainty arising from the autocorrelation in the residual.

3.2 Random Forest (RF) model

We have established a decision tree based random forest (RF) machine learning model to describe the relationships between hourly surface ozone concentrations (response variables) and their potential driving factors (predictive variables) in the urban areas over the QTP. As summarized in Table 2, predictive variables used in this study include time variables such as year 2015 to 2020, month 1 to 12, day of the year from 1 to 365, hour of the day from 0 to 23, and meteorological parameters such as wind, temperature, pressure, cloud fraction, rainfall, vertical transport, radiation and relative humidity. These time variables were selected as proxies for emissions since pollutant emissions vary by the time of day, day of the week, and season (Grange et al., 2018).

The detailed descriptions of RF machine learning model can be found in Breiman (Breiman, 2001). Briefly, the RF model is an ensemble model consisting of hundreds of individual decision tree models. Each individual decision tree model uses a bootstrap aggregating algorithm to randomly sample response variables and their predictive variables with a replacement from a training dataset. In this study, a single regression decision tree is grown in different decision rules based on the best fitting between surface ozone measurements and their predictive variables. The predictive variables are selected randomly to give the best split for each tree node. The predicted surface ozone concentrations are given by the final decision as the outcome of the weighted average

1 of all individual decision trees. By averaging all predictions from bootstrap samples, the bagging
2 process decreases variance and thus helps the model to minimize overfitting.

3   As shown in Figure 2, the whole dataset was randomly divided into (1) a training dataset to
4 establish the random forest model and (2) a testing dataset (not included in model training) to
5 evaluate the model performance. The training dataset was randomly selected from 70 % of the whole
6 data and the remaining 30% was taken as the testing dataset. The hyperparameters for the RF model
7 in this study were configured following those in Vu et al. (Vu et al., 2019) and Shi et al. (Shi et al.,
8 2021) and are summarized as follows: the maximum tree of a forest is 300 (n_tree=300), the number
9 of variables for splitting the decision tree is 4 (mtry=4), and the minimum size of terminal nodes is
10 3 (min_node_size=3). Since the meteorological variables differ in units and magnitudes, which
11 could lead to unstable performance of the model. Therefore, we uniformized all meteorological
12 variables via equation (1) before using them in the RF model. This pre-processing procedure can
13 also speed up the establishment of the RF model.

14
$$Z_k = \frac{x_k - u_k}{\sigma_k} \tag{3}$$

15 where u_k and σ_k are the average and 1σ standard deviation (STD) of x_k, and Z_k is the
16 pre-processed value for parameter x_k.

17 **3.3 Separation of meteorological and anthropologic contributions**
18   In order to separate the contributions of meteorology and anthropologic emission to surface
19 ozone anomalies in each city over the QTP, we have decoupled meteorology driven anomalies by
20 using the RF model based meteorological normalization method. The meteorological normalization
21 method was first introduced by (Grange et al., 2018) and improved by Vu et al. (Vu et al., 2019) and
22 Shi et al (Shi et al., 2021). To decouple the meteorological influence, we first generated a new input
23 dataset of predictive variables, which includes original time variables and resampled meteorological
24 variables ($T_{surface}$, U_{10}, V_{10}, PBLH, CLDT, PRECTOT, OMEGA, SWGDN, QV, TROPH).
25 Specifically, meteorological variables at a specific selected hour of a particular day in the input
26 dataset were generated by randomly selecting from the meteorological data during 1980 to 2020 at
27 that particular hour of different dates within a four-week period (i.e., 2 weeks before and 2 weeks
28 after that selected date). For example, the new input meteorological data at 18:00, 15 February 2018,
29 are randomly selected from the meteorological data at 18:00 on any date from 1 to 29 February of
30 any year during 1980 to 2020. This selection process was repeated 1000 times to generate a final
31 input dataset. The 1000 meteorological data were then fed to the RF model to predict surface ozone
32 concentration. The 1000 predicted ozone concentrations were then averaged as equation (4) to
33 calculate the final meteorological normalized concentration ($O_{3, dew}$) for that particular hour, day,
34 and year. This process ensures that all kinds of weather conditions around the measurement time
35 have been considered in the model predictions, which eliminate the influence of abnormal
36 meteorological conditions and get concentrations under the averaged meteorological conditions.

37
$$O_{3,dew} = \frac{1}{1000}\sum_{i=1}^{1000} O_{3,i,pred} \tag{4}$$

38 where $O_{3,i,pred}$ is the surface ozone concentration predicted by using the ith meteorological data
39 randomly selected from the meteorological data at the specific selected hour on any date from 1 to
40 29 February of any year in 1980 to 2020. $O_{3, dew}$ represents surface ozone concentration under the
41 mean meteorological conditions at the specific selected hour between 1980 to 2020.

If the seasonal variabilities of anthropogenic emission and meteorology are constant over year, the variability of surface <u>ozone</u> can be exactly reproduced by equation (2), i.e., the annual growth rate of surface ozone and the fitting residual should be close to zero. But this is not realistic in real world. Any year-to-year difference in either anthropogenic emission or meteorology could result in anomalies. We calculate surface ozone anomalies ($O_{3,anomalies}$) in each city over the QTP by subtracting their seasonal mean values ($O_{3,mean}$) from all hourly surface ozone measurements ($O_{3,individual}$) through equation (5) (Hakkarainen et al., 2019;Hakkarainen et al., 2016;Mustafa et al., 2021).

$$O_{3,anomalies} = O_{3,individual} - O_{3,mean} \tag{5}$$

where $O_{3,mean}$ in each city are approximated by the seasonality plus the intercept described in equation (1). As a result, the difference $O_{3,meteo}$ between $O_{3,individual}$ and $O_{3,dew}$ calculated as equation (6) is the portion of anomalies induced by changes in meteorology. The difference $O_{3,emis}$ between $O_{3,anomalies}$ and $O_{3,meteo}$ calculated as equation (7) represents the portion of anomalies induced by changes in anthropogenic emission.

$$O_{3,meteo} = O_{3,individual} - O_{3,dew} \tag{6}$$

$$O_{3,emis} = O_{3,anomalies} - O_{3,meteo} \tag{7}$$

By applying the meteorological normalization method, we finally separate the contributions of meteorology and anthropogenic emissions to the surface ozone anomalies in each city over the QTP. Positive $O_{3,meteo}$ and $O_{3,emis}$ indicate that changes in meteorology and anthropogenic emission cause surface ozone concentration above their seasonal mean values, respectively. Similarly, negative $O_{3,meteo}$ and $O_{3,emis}$ indicate that changes in meteorology and anthropogenic emission cause surface ozone concentration below their seasonal mean values, respectively.

4. Variabilities of surface ozone over the QTP
4.1 Overall ozone level

Statistical summary and box plot of surface ozone concentration (units: μg/m^3) in each city over the QTP from 2015 to 2020 are presented in <u>Table 3</u> and Figure S1, respectively. The average of surface ozone between 2015 and 2020 in each city over the QTP varied over (50.67 ±29.57) μg/m^3 to (90.38 ± 28.83) μg/m^3, and the median value varied over 53.00 μg/m^3 to 90.00 μg/m^3. In comparison, the averages of surface ozone between 2015 and 2020 in the Beijing-Tianjin-Hebei (BTH), the Fenwei Plain (FWP), the Yangtze River Delta (YRD) and the Pearl River Delta (PRD) in densely populated and highly industrialized eastern China were 140.76 μg/m^3, 132.16 μg/m^3, 125.09 μg/m^3 and 119.82 μg/m^3, respectively. The average of surface ozone between 2011 and 2015 at the suburb Nam Co station in the southern-central of the QTP was (47.00 ± 12.43) μg/m^3 (Yin et al., 2019b). As a result, surface ozone levels in the urban areas over the QTP are much lower than those in urban areas in eastern China but higher than those in the suburb areas over the QTP. Among all cities over the QTP, the highest and lowest surface ozone concentration occurs in Haixi and Aba, with mean values of (90.38 ± 28.83) μg/m^3 and (50.67 ± 28.83) μg/m^3, respectively. Generally, surface ozone concentrations in Qinghai province are higher than those in Tibet province. <u>We also presented the percentile variation of surface ozone concentration (units: μg/m^3) in each city over the QTP from 2015 to 2020 in Figure S2. The percentile variation modes of surface ozone concentration in all cities over the QTP are similar. In this study, only mean plus standard variance of surface ozone concentration rather than its percentile variation in each city was investigated. This prevailing method has been used in a number of studies to describe the variabilities of atmospheric</u>

compositions over the QTP (Li et al., 2020b;Liu et al., 2021;Ma et al., 2020;Xu et al., 2018;Xu et al., 2016;Yin et al., 2019c;Yin et al., 2017).

The ambient air quality standard issued by the Chinese government regularized that the critical value (Class 1 limit) for the maximum 8-hour average ozone level is 160 μg/m^3. With this rule, we summarize the number of nonattainment day per year in each city over the QTP in Table 3. The number of nonattainment day per city and per year over the QTP is only 2 between 2015 and 2020. Ozone nonattainment events over the QTP typically occur in spring or summer. In comparison, the number of nonattainment day per city and per year over the BTH, FWP, YRD and PRD are much larger, with values of 78, 36, 82 and 45 between 2015 and 2020, respectively, and all ozone nonattainment events over these regions occur in summer. The number of nonattainment day in Ngari in 2020, Lhasa in 2016 and 2017, Shannan in 2017 and 2018, Haixi in 2015 and 2019, and Xining in 2017 are 13, 10, 20, 12, 10, 14, 16, and 17 days, respectively. The number of nonattainment day in all other cities over the QTP are less than 10 days. Especially, surface ozone concentrations in Aba, Naqu, and Diqing in all years between 2015 and 2020 are less than the Class 1 limit of 160 μg/m^3. There are only 1 and 2 nonattainment days in Nyingchi and Qamdo between 2015 and 2020, respectively.

4.2 Diurnal variability

Diurnal cycles of surface ozone in each season and each city over the QTP are presented in Figure 3. Overall, diurnal cycle of surface ozone in each city over the QTP presents a unimodal pattern in all seasons. For all cities in all seasons, high levels of surface ozone occur in the daytime (9:00 to 20:00 LT) and low levels of surface ozone occur in the nighttime (21:00 to 08:00 LT). As seen from Figure 3, surface ozone levels usually increase over time starting at 8:00 to 11:00 LT in the morning, reach the maximum values at 15:00 to 18:00 LT in the afternoon, and then decreases over time till the minimum values at 8:00 or 9:00 LT the next day.

The timings of the diurnal cycles in all cities over the QTP were shifted by 1 to 2 hours later in winter than those in the rest of the year, most likely due to the later time of sunrise. Yin et al. (2017) also observed such shift in diurnal cycle at the suburb Nam Co station. The diurnal cycles of surface ozone in the urban areas over the QTP spanned a large range of −43.73 % to 47.12 % depending on region, season, and measurement time. The minimum and maximum surface ozone levels in the urban areas over the QTP varied over (22.89 ± 15.55) μg/m^3 to (68.96 ± 18.27) μg/m^3 and (57.77 ± 21.56) μg/m^3 to (102.08 ± 15.14) μg/m^3, respectively. On average, surface ozone levels in the urban areas over the QTP have mean values of (72.41 ± 33.83) μg/m^3 during the daytime (08:00-19:00) and (60.89 ± 32.25) μg/m^3 during the evening (20:00-08:00). The diurnal cycles of surface ozone in all cities over the QTP are generally consistent with the results reported in eastern China and the suburb areas over the QTP (Yin et al., 2019b;Yin et al., 2017;Zhao et al., 2016;Shen et al., 2014).

4.3 Seasonal variability

Monthly averaged time series of surface ozone in each city over the QTP between 2015 and 2020 are shown in Figure 4. Surface ozone levels in all cities over the QTP showed pronounced seasonal features. Seasonal cycles of surface ozone in most cities present a unimodal pattern with a seasonal peak occurs around March-July and a seasonal trough occurs around October-December. Specifically, maximum surface ozone levels occur in spring over Diqing, Lhasa, Naqu, Nyingchi, Qamdo, Shannan, Shigatse, Aba, and occur in summer over Ngari, Xining, Guoluo, and Haixi;

Minimum surface ozone levels in Nyingchi and Diqing occur in autumn, and in other cities occur in winter. The minimum and maximum surface ozone levels between 2015 and 2020 over the QTP varied over (29.21 ± 19.03) μg/m^3 to (60.45 ± 31.35) μg/m^3 and (71.25 ± 26.53) μg/m^3 to (112.46 ± 28.92) μg/m^3, respectively (Table S1). The peak−to−trough contrast in Diqing, Naqu, Nyingchi, and Aba were smaller than those in other cities. Due to regional deference in meteorology and anthropogenic emission, seasonal cycle of surface ozone in the urban areas over the QTP is also regional dependent.

4.4 Inter-annual variability

The inter-annual variability of surface ozone between 2015 and 2020 in each city over the QTP fitted by the bootstrap resampling method is presented in Figure 5 and S3, and also summarized in Table S1. Generally, the measured and fitted surface ozone concentrations in each city over the QTP are in good agreement with a correlation coefficient (R) of 0.68–0.92 (Figure S4). The measured features in terms of seasonality and inter-annual variability can be reproduced by the bootstrap resampling model. However, due to the year-to-year deference in anthropogenic emission and meteorology, both inter-annual variability and fitting residual were not zero in all cities. The inter-annual trends in surface ozone level from 2015 to 2020 over the QTP spanned a large range of (−2.43 ± 0.56) μg/m^3·yr^{-1} to (7.55 ± 1.61) μg/m^3·yr^{-1}, indicating a regional representation of each dataset. The inter-annual trends of surface ozone levels in most cities including Diqing, Naqu, Ngari, Nyingchi, Shannan, Shigatse, Xining, Abzhou and Haixi showed positive trends. The largest increasing trends were presented in Diqing and Nagri, with values of (5.31 ± 1.28) μg/m^3·yr^{-1} and (7.55 ± 1.61) μg/m^3·yr^{-1}, respectively. In contrast, surface ozone levels in Lhasa, Qamdo and Guoluo presented negative trends, with values of (-1.62 ± 0.76) μg/m^3·yr^{-1}, (-2.43 ± 0.56) μg/m^3·yr^{-1} and (-2.36 ± 0.81) μg/m^3·yr^{-1}, respectively.

5. Performance evaluation

We evaluate the performance of the RF model in predicting hourly surface ozone level in each city over the QTP using the metrics of Pearson correlation coefficient (R), the root means square error (RMSE), and the mean absolute error (MAE). They are commonly used metrics for evaluation of machine learning model predictions, and are defined as equations (8), (9), and (10), respectively.

$$R = \frac{n\sum_{i=0}^{n} x_i y_i - \sum_{i=0}^{n} x_i \cdot \sum_{i=0}^{n} y_i}{\sqrt{n\sum_{i=0}^{n} x_i^2 - \left(\sum_{i=0}^{n} x_i\right)^2} \cdot \sqrt{n\sum_{i=0}^{n} y_i^2 - \left(\sum_{i=0}^{n} y_i\right)^2}} \tag{8}$$

$$RMSE = \sqrt{\frac{\sum_{i=1}^{n}(x_i - y_i)^2}{n}} \tag{9}$$

$$MAE = \frac{\sum_{i=1}^{n}|x_i - y_i|}{n} \tag{10}$$

where x_i and y_i are the ith concurrent measured and predicted data pairs, respectively. The n is the number of measurements. The R value represents the fitting correlation between the measurements and predictions. The RMSE value measures the relative average difference between the measurements and predictions. The MAE value measures the absolute average difference between the measurements and predictions. The units of RMSE and MAE are same as the measured data, namely μg/m^3.

Comparisons between the model predictions and measurements for the testing data (not included in model training) in each city over the QTP are shown in Figure S5. Overall, the RF model

predictions and surface ozone measurements are in good agreements, showing high R and low RMSE and MAE for testing dataset in each city over the QTP (Figure S5). Depending on cities, the R values varied over 0.85 to 0.94, the RMSE over 10.24 to 17.55 μg/m^3, and MAE over 7.32 to 12.76 μg/m^3. The R, RMSE, and MAE are independent of city and surface ozone level. The results affirm that our model performs very well in predicting surface ozone levels and variabilities in each city over the QTP.

We further investigate the importance of each input variable in the RF model for predicting surface ozone level in each city over the QTP. As shown in Figure S6, time information such as hour term (Hour), year term (Year) or seasonal term (Month) are the most important variables in the RF model predictions in all cities except Xining and Haixi where temperature term (T_{2m}) is the most important variable. For all cities, the aggregate importance of time information is larger than 50%. In all cities over the QTP, the meteorological variables such as temperature (T_{2m}), relatively humidity (QV), Vertical pressure velocity (OMEGA) and Planetary boundary layer height (PBLH) play significant roles when explaining surface ozone concentrations. For other variables, although they are not decisive variables in the RF model predictions, they are not negligible in predicting surface ozone in all cities over the QTP. Although time information are the most important variables in the RF model predictions, they can be used very precisely, and thus the RF model to measurement discrepancy in all cities could be from other predictive variables rather than time information.

6. Drivers of surface ozone anomalies

In this section, we explore the drivers of surface ozone anomalies between 2015 and 2020 over the QTP. We first present descriptively the contributions of anthropogenic emission and meteorology to surface ozone anomalies over the QTP in section 6.1 to 6.3, where statistics on different time scales were summarized. We then present in-depth analysis of each driver in section 6.4.

6.1 Diurnal scale

Figure 6 presents diurnal cycles of surface ozone anomalies between 2015 and 2020 along with the meteorology-driven and anthropogenic-driven portions in each city over the QTP. In all cities, the anthropogenic contributions are almost constant but the meteorological contributions show large variations throughout the day. Depending on region and measurement hour, diurnal surface ozone anomalies on average varied over -27.82 μg/m^3 to 37.11 μg/m^3 between 2015 and 2020, where meteorological and anthropogenic contributions varied over -33.88 μg/m^3 to 35.86 μg/m^3 and -4.32 μg/m^3 to 4.05 μg/m^3, respectively. The least contrast between meteorological contribution and anthropogenic contribution occurs in Haixi. The diurnal cycles of meteorological contribution are consistent with those of surface ozone anomalies. High levels of meteorological contribution occur in the daytime (9:00 to 20:00 LT) and low levels of meteorological contributions occur in the nighttime. As a result, diurnal surface ozone anomalies in each city over the QTP were mainly driven by meteorology.

We further investigated the drivers of surface ozone nonattainment events from 2015 to 2020 in each city over the QTP. All ozone nonattainment events were classified as meteorology-dominated or anthropogenic-dominated events according to which one has a larger contribution to the observed surface ozone nonattainment events. The statistical results are listed in Table S2. Except one day in Ngari in 2018, one day in Shigatse in 2016, and one day in Haixi in 2019 which

were dominated by anthropogenic emission, all other surface ozone nonattainment events from 2015 to 2020 over the QTP were dominated by meteorology. Exceptional meteorology driven 97% of surface ozone nonattainment events from 2015 to 2020 in the urban areas over the QTP. For the meteorology-dominated surface ozone nonattainment events, meteorological and anthropogenic contributions varied over 32.85 μg/m^3 to 55.61 μg/m^3 and 3.67 μg/m^3 to 7.23 μg/m^3, respectively. For the anthropogenic-dominated surface ozone nonattainment events, meteorological and anthropogenic contributions varied over 7.63 μg/m^3 to 10.53 μg/m^3 and 15.63 μg/m^3 to 35.28 μg/m^3, respectively.

6.2 Seasonal scale

Figure 7 presents seasonal cycles of surface ozone anomalies between 2015 and 2020 along with the meteorology-driven and anthropogenic-driven portions in each city over the QTP. In all cities, the monthly averaged surface ozone anomalies between 2015 and 2020 varied with much smaller amplitudes than their diurnal anomalies. Noticeable anomalies include pronounced positive anomalies in December in Nagri, in May in Lhasa, Shannan, and Qamdo, in July in Haixi, in June in Guoluo, and negative anomalies in July in Lhasa, Nyingchi, and Guoluo. Both meteorological and anthropogenic contributions are regional dependent and show large variations throughout the year. Depending on region and month, meteorological and anthropogenic contributions varied over -4.54 μg/m^3 to 3.31 μg/m^3 and -2.67 μg/m^3 to 3.35 μg/m^3 between 2015 and 2020, respectively.

Seasonal surface ozone anomalies between 2015 and 2020 in all cities over the QTP were mainly driven by meteorology. For example, meteorology caused decrements of 3.05 μg/m^3 in July and 4.27 μg/m^3 in September in Diqing, while anthropogenic emission caused increments of 0.64 μg/m^3 and 1.34 μg/m^3 in respective months. Aggregately, we observed -2.41 μg/m^3 and -2.89 μg/m^3 of seasonal surface ozone anomalies in July and September in Ngari, respectively. In all cities, seasonal cycles of meteorological contribution are more consistent with those of surface ozone anomalies over the QTP. In some cases, surface ozone anomalies would have larger values if not for the unfavorable meteorological conditions, e.g., surface ozone anomalies in June in Ngari, in December in Shannan, Guoluo and Aba.

6.3 Multi-year scale

Annual mean surface ozone anomalies between 2015 and 2020 along with meteorology-driven and anthropogenic-driven portions in each city over the QTP are presented in Figure 8. Surface ozone in Diqing, Naqu, Nagri, Haixi and Shannan show larger year to year variations than those in other cities. Annual mean surface ozone levels in Diqing, Naqu, Nagri and Haixi showed significant reductions of 2.10 μg/m^3, 10.32 μg/m^3, 6.87 μg/m^3, and 15.97 μg/m^3, respectively, Shannan showed an increment of 9.12 μg/m^3, and other cities showed comparable values in 2016 relative to 2015. The largest year to year difference occurred in Ngari during 2016 to 2017, which has an increment of 25.25 μg/m^3. The results show that anthropogenic contributions decreased by 1.85 μg/m^3, 7.14 μg/m^3, 5.65 μg/m^3, and 15.98 μg/m^3, respectively, in Diqing, Naqu, Nagri, Haixi, and increased by 11.13 μg/m^3 in Shannan in 2016 relative to 2015, and increased by 20.85 μg/m^3 in Ngari in 2017 relative to 2016. As a result, all above reductions or increments in surface ozone level were mainly driven by anthropogenic emission. In contrast, surface ozone anomalies in Lhasa in 2017 and 2020, in Shigatse and Nyingchi in 2019 were mainly driven by meteorology.

Table S3 summarizes the inter-annual trends of surface ozone anomalies, meteorological and

anthropogenic contributions from 2015 to 2020 in each city over the QTP. Except Guoluo, Qamdo and Lhasa which show decreasing trends, anthropogenic contributions in all other cities showed increasing trends from 2015 to 2020. With respect to meteorology contribution, Ngari, Naqu, Diqing and Haixi showed increasing trends from 2015 to 2020 and all other cities showed decreasing trends. The inter-annual trends of surface ozone anomalies in Ngari, Lhasa, Naqu, Qamdo, Diqing, Haixi and Guoluo can be attributed to anthropogenic emissions by 95.77%, 96.30%, 97.83%, 82.30%, 99.26%, and 87.85%, and meteorology by 4.23%, 3.70%, 2.17%, 3.19%, 0.74%, and 12.15%, respectively. The inter-annual trends of surface ozone in other cities were fully driven by anthropogenic emission, where the increasing inter-annual trends would have larger values if not for the favorable meteorological conditions. As a result, the inter-annual trends of surface ozone anomalies in all cities over the QTP were dominated by anthropogenic emission.

6.4 Discussions

Typically, all cities over the QTP are formed at flat valleys with surrounding mountains rising to more than 5.0 km a.s.l., and keep continuous expansion and development over time. Inhibited by surrounding mountains, regional dependent emissions and mountain peak-valley meteorological systems result in regional representation of surface ozone level and their drivers on diurnal, seasonal, inter-annual scales.

Correlations between $O_{3,meteo}$ and each meteorological anomaly are summarized for all time, diurnal scale, seasonal scale and multi-year scale in Table S4-S7. We find that all time scales of meteorology-driven surface ozone anomalies in each city are positively related with anomalies of temperature, planetary boundary layer height (PBLH), surface incoming shortwave flux (SWGDN), downward transport velocity at the PBLH (OMEGA), and tropopause height (TROPH). Among all these positive correlations, the correlations with temperature, PBLH, and SWGDN in all cities are higher than those with OMEGA and TROPH. Since high temperature and SWGDN facilitate the formation of ozone via the increase in chemical reaction rates or biogenic emissions, the meteorology-driven surface ozone anomalies have the highest correlations with the changes in temperature and SWGDN. Possible reasons for the ozone increases with the increase in PBLH include lower NO concentration at the urban surface due to the deep vertical mixing, which then limits ozone destruction and increases ozone concentrations (He et al., 2017), and more downward transport of ozone from the free troposphere where the ozone concentration is higher than the near-surface concentration (Sun et al., 2009). Large OMEGA and high tropopause height also facilitate downward transport of stratospheric ozone, resulting in high surface ozone level. The QTP has been identified as a hot spot for stratospheric–tropospheric exchange (Cristofanelli et al., 2010;Škerlak et al., 2014) where the surface ozone is elevated from the baseline during the spring due to frequent stratospheric intrusions. Generally, surface ozone anomalies are negatively related with humidity, rainfall, and total cloud fraction in each city over the QTP. These wet meteorological conditions inhibit biogenic emissions, slow down ozone chemical production, and facilitate the ventilation of ozone and its precursors (Gong and Liao, 2019;Jiang et al., 2021;Lu et al., 2019a;Lu et al., 2019b;Ma et al., 2019), and therefore contribute to ozone decrease.

The U_{10m} and V_{10m} represent the metrics for evaluating the horizontal transport. In most of cities over QTP, noticeable ozone vs. horizontal wind correlations are observed, indicating that horizontal transport is an important contributor to surface ozone (Shen et al., 2014;Zhu et al., 2004). The QTP region, as a whole, is primarily regulated by the interplay of the Indian summer monsoon

and the westerlies, and the atmospheric environment over QTP is heterogeneous. Mount Everest is representative of the Himalayas on the southern edge of the Tibetan Plateau and is close to South Asia where anthropogenic atmospheric pollution has been increasingly recognized as disturbing the high mountain regions (Decesari et al., 2010;Maione et al., 2011;Putero et al., 2014). In the northern QTP, including Xining, Haixi and Guoluo, is occasionally influenced by regional polluted air masses (Xue et al., 2011;Zhu et al., 2004), especially, the impacts of anthropogenic emissions from central and eastern China in the summer (Xue et al., 2011). For cities over the inland QTP, is distant from both South Asia and northwestern China; it has been found to be influenced by episodic long-range transport of air pollution from South Asia (Lüthi et al., 2015), evidenced by the study of aerosol and precipitation chemistry at these cities (Cong et al., 2010).

In order to determine which specific meteorological variables responsible for the meteorology-dominated ozone nonattainment events over the QTP, we have investigated the correlations between each meteorological variable and ozone anomalies in each city during the ozone nonattainment days. As tabulated in Table S8, temperature is the dominant meteorological variable responsible for the meteorology-dominated ozone nonattainment events, especially in Shigatse, Lhasa, Shannan, Haixi and Guoluo. In addition, the OMEGA is also an important meteorological variable in most cities, especially in Guoluo where the correlation is up to 0.69. For other meteorological variables, winds (U10m, V10m) and TROPH also have noticeable contributions to some ozone nonattainment events.

The NO_x and VOCs are main precursors of surface ozone. The monthly and annual averaged anthropogenic emissions of NO_x and VOCs in each city over the QTP extracted from the MEIC (Multi-resolution Emission Inventory for China) inventory between 2015 to 2017 are presented in Table S9-S12. Major anthropogenic emissions in each city over the QTP are from transport sector and residential sector including burning emissions of coal, post-harvest crop residue, yak dung and religious incense (Chen et al., 2009;Kang et al., 2016;Kang et al., 2019;Li et al., 2017). The NO_x and VOCs emissions have been decreased in Diqing, Naqu, Nagri in 2016 relative to 2015. These reductions of NO_x and VOCs emissions jointly driven the changes of ozone in these cities. Although NO_x emissions increased in Haixi during 2015 to 2016, VOCs emissions have significantly decreased by 6.82 t. As a result, the decreases of ozone in Haixi in 2016 relative to 2015 were attributed to VOCs reductions in the same period.

The correlations of the monthly and annual averaged anthropogenic contributions against the NO_x and VOCs emissions are summarized in Table S13. The correlations of the monthly averaged anthropogenic contributions against anthropogenic NO_x and VOCs emissions are in the range of 0.35-0.81 and 0.33-0.83, respectively. For the annual averaged statistics, the correlations against NO_x and VOCs emissions are in the range of 0.15-0.94 (expect for Nyingchi and Diqing), and 0.34-0.98 (expect for Haixi), respectively. For all cities except Shannan, Qamdo and Haixi, both the NO_x and VOCs emissions are consistent with the anthropogenic contributions. While only NO_x emissions in Qamdo and Haixi and VOCs emissions in Shannan are consistent with anthropogenic contributions. In general, the changes of NO_x and VOCs emissions in MEIC inventory are able to explain the variabilities of both monthly and annual averaged anthropogenic contributions.

7. Conclusions

In this study, we have investigated the evolutions, implications, and the drivers of surface ozone anomalies (defined as deviations of ozone levels relative to their seasonal means) between 2015 and 2020 in the urban areas over the QTP. Diurnal, seasonal, and inter annual variabilities of surface

ozone in 12 cities over the QTP are analyzed. The average of surface ozone between 2015 and 2020 in each city over the QTP varied over (50.67 ± 29.57) μg/m^3 to (90.38 ± 28.83) μg/m^3, and the median value varied over 53.00 μg/m^3 to 90.00 μg/m^3. Overall, diurnal cycle of surface ozone in each city over the QTP presents a unimodal pattern in all seasons. For all cities in all seasons, high levels of surface ozone occur in the daytime (9:00 to 20:00 LT) and low levels of surface ozone occur in the nighttime (21:00 to 08:00 LT). Seasonal cycles of surface ozone in most cities present a unimodal pattern with a seasonal peak occurs around March-July and a seasonal trough occurs around October-December. The inter-annual trends in surface ozone level from 2015 to 2020 over the QTP spanned a large range of (-2.43 ± 0.56) μg/m^3·yr^{-1} to (7.55 ± 1.61) μg/m^3·yr^{-1}, indicating a regional representation of each dataset.

We have established a RF regression model to describe the relationships between hourly surface ozone concentrations (response variables) and their potential driving factors (predictive variables) in the urban areas over the QTP. The RF model predictions and surface ozone measurements are in good agreement, showing high R and low RMSE and MAE in each city over the QTP. Depending on cities, the R values varied over 0.85 to 0.94, the RMSE over 10.24 to 17.55 μg/m^3, and MAE over 7.32 to 12.76 μg/m^3. The R, RMSE, and MAE are independent of city and surface ozone level. The results affirm that our model performs very well in predicting surface ozone levels and variabilities in each city over the QTP.

We have separated quantitatively the contributions of anthropogenic emission and meteorology to surface ozone anomalies by using the RF model based meteorological normalization method. Diurnal and seasonal surface ozone anomalies over the QTP were mainly driven by meteorology, and inter-annual anomalies were mainly driven by anthropogenic emission. Depending on region and measurement hour, diurnal surface ozone anomalies varied over -30.55 μg/m^3 to 34.01 μg/m^3 between 2015 and 2020, where meteorological and anthropogenic contributions varied over -20.08 μg/m^3 to 48.73 μg/m^3 and -27.18 μg/m^3 to 1.92 μg/m^3, respectively. Unfavorable meteorology driven 97% of surface ozone nonattainment events between 2015 and 2020 in the urban areas over the QTP. Monthly averaged surface ozone anomalies varied with much smaller amplitudes than their diurnal anomalies, where meteorological and anthropogenic contributions varied over 7.63 μg/m^3 to 55.61 μg/m^3 and 3.67 μg/m^3 to 35.28 μg/m^3 between 2015 and 2020, respectively. The inter-annual trends of surface ozone anomalies in Ngari, Lhasa, Naqu, Qamdo, Diqing, Haixi and Guoluo can be attributed to anthropogenic emissions by 95.77%, 96.30%, 97.83%, 82.30%, 99.26%, and 87.85%, and meteorology by 4.23%, 3.70%, 2.17%, 3.19%, 0.74%, and 12.15%, respectively. The inter-annual trends of surface ozone anomalies in other cities were fully driven by anthropogenic emission, where the increasing inter-annual trends would have larger values if not for the favorable meteorological conditions. This study can not only improve our knowledge with respect to spatiotemporal variability of surface ozone but also provides valuable implication for ozone mitigation over the QTP.

Author contributions. HY designed the study and wrote the paper. YS supervised and revised this paper. JN, MP, CY and CL provided constructive comments.

1   *Competing interests.* None.

5

1 **Reference**

2 Breiman, L.: Random Forests, Machine Learning, 45, 5-32, 10.1023/A:1010933404324, 2001.

3 Carvalho, D.: An Assessment of NASA's GMAO MERRA-2 Reanalysis Surface Winds, J Climate, 32,
4   8261-8281, 10.1175/JCLI-D-19-0199.1, 2019.

5 Chen, D., Wang, Y., McElroy, M. B., He, K., Yantosca, R. M., and Le Sager, P.: Regional CO pollution
6   and export in China simulated by the high-resolution nested-grid GEOS-Chem model, Atmos Chem
7   Phys, 9, 3825-3839, 2009.

8 Cong, Z., Kang, S., Zhang, Y., and Li, X.: Atmospheric wet deposition of trace elements to central Tibetan
9   Plateau, Applied Geochemistry, 25, 1415-1421, https://doi.org/10.1016/j.apgeochem.2010.06.011,
10   2010.

11 Cristofanelli, P., Bracci, A., Sprenger, M., Marinoni, A., Bonafè, U., Calzolari, F., Duchi, R., Laj, P.,
12   Pichon, J. M., Roccato, F., Venzac, H., Vuillermoz, E., and Bonasoni, P.: Tropospheric ozone
13   variations at the Nepal Climate Observatory-Pyramid (Himalayas, 5079 m a.s.l.) and influence of
14   deep stratospheric intrusion events, Atmos. Chem. Phys., 10, 6537-6549, 10.5194/acp-10-6537-
15   2010, 2010.

16 Decesari, S., Facchini, M. C., Carbone, C., Giulianelli, L., Rinaldi, M., Finessi, E., Fuzzi, S., Marinoni,
17   A., Cristofanelli, P., Duchi, R., Bonasoni, P., Vuillermoz, E., Cozic, J., Jaffrezo, J. L., and Laj, P.:
18   Chemical composition of PM_{10} and PM_1 at the high-altitude Himalayan station Nepal Climate
19   Observatory-Pyramid (NCO-P) (5079 m a.s.l.), Atmos. Chem. Phys., 10, 4583-4596, 10.5194/acp-
20   10-4583-2010, 2010.

21 Duo, B., Cui, L. L., Wang, Z. Z., Li, R., Zhang, L. W., Fu, H. B., Chen, J. M., Zhang, H. F., and Qiong,
22   A.: Observations of atmospheric pollutants at Lhasa during 2014-2015: Pollution status and the
23   influence of meteorological factors, J Environ Sci, 63, 28-42, 2018.

24 Gardiner, T., Forbes, A., de Maziere, M., Vigouroux, C., Mahieu, E., Demoulin, P., Velazco, V., Notholt,
25   J., Blumenstock, T., Hase, F., Kramer, I., Sussmann, R., Stremme, W., Mellqvist, J., Strandberg, A.,
26   Ellingsen, K., and Gauss, M.: Trend analysis of greenhouse gases over Europe measured by a
27   network of ground-based remote FTIR instruments, Atmos Chem Phys, 8, 6719-6727, 2008.

28 Gardner, M., and Dorling, S.: Artificial Neural Network-Derived Trends in Daily Maximum Surface
29   Ozone Concentrations, Journal of the Air & Waste Management Association, 51, 1202-1210,
30   10.1080/10473289.2001.10464338, 2001.

31 Gelaro, R., McCarty, W., Suárez, M. J., Todling, R., Molod, A., Takacs, L., Randles, C. A., Darmenov,
32   A., Bosilovich, M. G., Reichle, R., Wargan, K., Coy, L., Cullather, R., Draper, C., Akella, S.,
33   Buchard, V., Conaty, A., da Silva, A. M., Gu, W., Gi-Kong, K., Koster, R., Lucchesi, R., Merkova,
34   D., Nielsen, J. E., Partyka, G., Pawson, S., Putman, W., Rienecker, M., Schubert, S. D., Sienkiewicz,
35   M., and Zhao, B.: The Modern-Era Retrospective Analysis for Research and Applications, Version
36   2 (MERRA-2), J Climate, 30, 5419-5454, http://dx.doi.org/10.1175/JCLI-D-16-0758.1, 2017.

37 Gong, C., and Liao, H.: A typical weather pattern for ozone pollution events in North China, Atmos.
38   Chem. Phys., 19, 13725-13740, 10.5194/acp-19-13725-2019, 2019.

39 Grange, S. K., Carslaw, D. C., Lewis, A. C., Boleti, E., and Hueglin, C.: Random forest meteorological
40   normalisation models for Swiss PM_{10} trend analysis, Atmos Chem Phys, 18, 6223-6239, 2018.

41 Grange, S. K., and Carslaw, D. C.: Using meteorological normalisation to detect interventions in air
42   quality time series, Sci Total Environ, 653, 578-588, 2019.

43 Hakkarainen, J., Ialongo, I., and Tamminen, J.: Direct space-based observations of anthropogenic CO_2
44   emission   areas   from   OCO-2,   Geophys   Res   Lett,   43,   11,400-411,406,

https://doi.org/10.1002/2016GL070885, 2016.

Hakkarainen, J., Ialongo, I., Maksyutov, S., and Crisp, D.: Analysis of Four Years of Global XCO_2 Anomalies as Seen by Orbiting Carbon Observatory-2, Remote Sens-Basel, 11, 10.3390/rs11070850, 2019.

He, J., Gong, S., Yu, Y., Yu, L., Wu, L., Mao, H., Song, C., Zhao, S., Liu, H., Li, X., and Li, R.: Air pollution characteristics and their relation to meteorological conditions during 2014–2015 in major Chinese cities, Environmental Pollution, 223, 484-496, https://doi.org/10.1016/j.envpol.2017.01.050, 2017.

Hou, L. L., Dai, Q. L., Song, C. B., Liu, B. W., Guo, F. Z., Dai, T. J., Li, L. X., Liu, B. S., Bi, X. H., Zhang, Y. F., and Feng, Y. C.: Revealing Drivers of Haze Pollution by Explainable Machine Learning, Environ Sci Tech Let, 9, 112-119, 2022.

Immerzeel, W. W., van Beek, L. P. H., and Bierkens, M. F. P.: Climate Change Will Affect the Asian Water Towers, Science, 328, 1382-1385, 2010.

Jerrett, M., Burnett, R. T., Pope, C. A., Ito, K., Thurston, G., Krewski, D., Shi, Y., Calle, E., and Thun, M.: Long-Term Ozone Exposure and Mortality, New Engl J Med, 360, 1085-1095, 10.1056/NEJMoa0803894, 2009.

Jiang, Z., Li, J., Lu, X., Gong, C., Zhang, L., and Liao, H.: Impact of western Pacific subtropical high on ozone pollution over eastern China, Atmos. Chem. Phys., 21, 2601-2613, 10.5194/acp-21-2601-2021, 2021.

Kang, S. C., Huang, J., Wang, F. Y., Zhang, Q. G., Zhang, Y. L., Li, C. L., Wang, L., Chen, P. F., Sharma, C. M., Li, Q., Sillanpaa, M., Hou, J. Z., Xu, B. Q., and Guo, J. M.: Atmospheric Mercury Depositional Chronology Reconstructed from Lake Sediments and Ice Core in the Himalayas and Tibetan Plateau, Environmental Science & Technology, 50, 2859-2869, 2016.

Kang, S. C., Zhang, Q. G., Qian, Y., Ji, Z. M., Li, C. L., Cong, Z. Y., Zhang, Y. L., Guo, J. M., Du, W. T., Huang, J., You, Q. L., Panday, A. K., Rupakheti, M., Chen, D. L., Gustafsson, O., Thiemens, M. H., and Qin, D. H.: Linking atmospheric pollution to cryospheric change in the Third Pole region: current progress and future prospects, Natl Sci Rev, 6, 796-809, 2019.

Kishore Kumar, G., Kishore Kumar, K., Baumgarten, G., and Ramkumar, G.: Validation of MERRA reanalysis upper-level winds over low latitudes with independent rocket sounding data, J Atmos Sol-Terr Phy, 123, 48-54, https://doi.org/10.1016/j.jastp.2014.12.001, 2015.

Li, K., Jacob, D. J., Liao, H., Shen, L., Zhang, Q., and Bates, K. H.: Anthropogenic drivers of 2013–2017 trends in summer surface ozone in China, Proceedings of the National Academy of Sciences, 116, 422, 10.1073/pnas.1812168116, 2019.

Li, K., Jacob, D. J., Shen, L., Lu, X., De Smedt, I., and Liao, H.: Increases in surface ozone pollution in China from 2013 to 2019: anthropogenic and meteorological influences, Atmos. Chem. Phys., 20, 11423-11433, 10.5194/acp-20-11423-2020, 2020a.

Li, M., Zhang, Q., Kurokawa, J., Woo, J. H., He, K. B., Lu, Z. F., Ohara, T., Song, Y., Streets, D. G., Carmichael, G. R., Cheng, Y. F., Hong, C. P., Huo, H., Jiang, X. J., Kang, S. C., Liu, F., Su, H., and Zheng, B.: MIX: a mosaic Asian anthropogenic emission inventory under the international collaboration framework of the MICS-Asia and HTAP, Atmos Chem Phys, 17, 935-963, 10.5194/acp-17-935-2017, 2017.

Li, R., Zhao, Y. L., Zhou, W. H., Meng, Y., Zhang, Z. Y., and Fu, H. B.: Developing a novel hybrid model for the estimation of surface 8 h ozone (O_3) across the remote Tibetan Plateau during 2005-2018, Atmos Chem Phys, 20, 6159-6175, 2020b.

Liu, S., Fang, S. X., Liu, P., Liang, M., Guo, M. R., and Feng, Z. Z.: Measurement report: Changing characteristics of atmospheric CH_4 in the Tibetan Plateau: records from 1994 to 2019 at the Mount Waliguan station, Atmos Chem Phys, 21, 393-413, 10.5194/acp-21-393-2021, 2021.

Loewen, M., Kang, S., Armstrong, D., Zhang, Q., Tomy, G., and Wang, F.: Atmospheric transport of mercury to the Tibetan plateau, Environmental Science & Technology, 41, 7632-7638, 2007.

Lu, X., Hong, J., Zhang, L., Cooper, O. R., Schultz, M. G., Xu, X., Wang, T., Gao, M., Zhao, Y., and Zhang, Y.: Severe Surface Ozone Pollution in China: A Global Perspective, Environ Sci Tech Let, 5, 487-494, 10.1021/acs.estlett.8b00366, 2018.

Lu, X., Zhang, L., Chen, Y., Zhou, M., Zheng, B., Li, K., Liu, Y., Lin, J., Fu, T. M., and Zhang, Q.: Exploring 2016–2017 surface ozone pollution over China: source contributions and meteorological influences, Atmos. Chem. Phys., 19, 8339-8361, 10.5194/acp-19-8339-2019, 2019a.

Lu, X., Zhang, L., and Shen, L.: Meteorology and Climate Influences on Tropospheric Ozone: a Review of Natural Sources, Chemistry, and Transport Patterns, Current Pollution Reports, 5, 238-260, 10.1007/s40726-019-00118-3, 2019b.

Lu, X., Zhang, L., Wang, X., Gao, M., Li, K., Zhang, Y., Yue, X., and Zhang, Y.: Rapid Increases in Warm-Season Surface Ozone and Resulting Health Impact in China Since 2013, Environ Sci Tech Let, 7, 240-247, 10.1021/acs.estlett.0c00171, 2020.

Lu, X., Ye, X., Zhou, M., Zhao, Y., Weng, H., Kong, H., Li, K., Gao, M., Zheng, B., Lin, J., Zhou, F., Zhang, Q., Wu, D., Zhang, L., and Zhang, Y.: The underappreciated role of agricultural soil nitrogen oxide emissions in ozone pollution regulation in North China, Nature Communications, 12, 5021, 10.1038/s41467-021-25147-9, 2021.

Lüthi, Z. L., Škerlak, B., Kim, S. W., Lauer, A., Mues, A., Rupakheti, M., and Kang, S.: Atmospheric brown clouds reach the Tibetan Plateau by crossing the Himalayas, Atmos. Chem. Phys., 15, 6007-6021, 10.5194/acp-15-6007-2015, 2015.

Ma, J., Dörner, S., Donner, S., Jin, J., Cheng, S., Guo, J., Zhang, Z., Wang, J., Liu, P., Zhang, G., Pukite, J., Lampel, J., and Wagner, T.: MAX-DOAS measurements of NO_2, SO_2, HCHO, and BrO at the Mt. Waliguan WMO GAW global baseline station in the Tibetan Plateau, Atmos. Chem. Phys., 20, 6973-6990, 10.5194/acp-20-6973-2020, 2020.

Ma, M., Gao, Y., Wang, Y., Zhang, S., Leung, L. R., Liu, C., Wang, S., Zhao, B., Chang, X., Su, H., Zhang, T., Sheng, L., Yao, X., and Gao, H.: Substantial ozone enhancement over the North China Plain from increased biogenic emissions due to heat waves and land cover in summer 2017, Atmos. Chem. Phys., 19, 12195-12207, 10.5194/acp-19-12195-2019, 2019.

Maione, M., Giostra, U., Arduini, J., Furlani, F., Bonasoni, P., Cristofanelli, P., Laj, P., and Vuillermoz, E.: Three-year observations of halocarbons at the Nepal Climate Observatory at Pyramid (NCO-P, 5079 m a.s.l.) on the Himalayan range, Atmos. Chem. Phys., 11, 3431-3441, 10.5194/acp-11-3431-2011, 2011.

Mustafa, F., Bu, L., Wang, Q., Yao, N., Shahzaman, M., Bilal, M., Aslam, R. W., and Iqbal, R.: Neural-network-based estimation of regional-scale anthropogenic CO_2 emissions using an Orbiting Carbon Observatory-2 (OCO-2) dataset over East and West Asia, Atmos. Meas. Tech., 14, 7277-7290, 10.5194/amt-14-7277-2021, 2021.

Pu, Z. X., Xu, L., and Salomonson, V. V.: MODIS/Terra observed seasonal variations of snow cover over the Tibetan Plateau, Geophys Res Lett, 34, 2007.

Putero, D., Landi, T. C., Cristofanelli, P., Marinoni, A., Laj, P., Duchi, R., Calzolari, F., Verza, G. P., and Bonasoni, P.: Influence of open vegetation fires on black carbon and ozone variability in the

southern Himalayas (NCO-P, 5079 m a.s.l.), Environmental Pollution, 184, 597-604, https://doi.org/10.1016/j.envpol.2013.09.035, 2014.

Qiu, J.: The third pole, Nature, 454, 393-396, 2008.

Santer, B. D., Thorne, P. W., Haimberger, L., Taylor, K. E., Wigley, T. M. L., Lanzante, J. R., Solomon, S., Free, M., Gleckler, P. J., Jones, P. D., Karl, T. R., Klein, S. A., Mears, C., Nychka, D., Schmidt, G. A., Sherwood, S. C., and Wentz, F. J.: Consistency of modelled and observed temperature trends in the tropical troposphere, Int J Climatol, 28, 1703-1722, 2008.

Shen, Z., Cao, J., Zhang, L., Zhao, Z., Dong, J., Wang, L., Wang, Q., Li, G., Liu, S., and Zhang, Q.: Characteristics of surface O_3 over Qinghai Lake area in Northeast Tibetan Plateau, China, Sci Total Environ, 500-501, 295-301, https://doi.org/10.1016/j.scitotenv.2014.08.104, 2014.

Shi, Z. B., Song, C. B., Liu, B. W., Lu, G. D., Xu, J. S., Vu, T. V., Elliott, R. J. R., Li, W. J., Bloss, W. J., and Harrison, R. M.: Abrupt but smaller than expected changes in surface air quality attributable to COVID-19 lockdowns, Sci Adv, 7, 2021.

Škerlak, B., Sprenger, M., and Wernli, H.: A global climatology of stratosphere–troposphere exchange using the ERA-Interim data set from 1979 to 2011, Atmos. Chem. Phys., 14, 913-937, 10.5194/acp-14-913-2014, 2014.

Song, Z., Fu, D., Zhang, X., Wu, Y., Xia, X., He, J., Han, X., Zhang, R., and Che, H.: Diurnal and seasonal variability of PM2.5 and AOD in North China plain: Comparison of MERRA-2 products and ground measurements, Atmos Environ, 191, 70-78, https://doi.org/10.1016/j.atmosenv.2018.08.012, 2018.

Sun, Y., Wang, Y., and Zhang, C.: Vertical observations and analysis of $PM_{2.5}$, O_3, and NO_x at Beijing and Tianjin from towers during summer and Autumn 2006, Advances in Atmospheric Sciences, 27, 123, 10.1007/s00376-009-8154-z, 2009.

Sun, Y., Liu, C., Zhang, L., Palm, M., Notholt, J., Yin, H., Vigouroux, C., Lutsch, E., Wang, W., Shan, C., Blumenstock, T., Nagahama, T., Morino, I., Mahieu, E., Strong, K., Langerock, B., De Mazière, M., Hu, Q., Zhang, H., Petri, C., and Liu, J.: Fourier transform infrared time series of tropospheric HCN in eastern China: seasonality, interannual variability, and source attribution, Atmos. Chem. Phys., 20, 5437-5456, 10.5194/acp-20-5437-2020, 2020.

Sun, Y., Yin, H., Liu, C., Mahieu, E., Notholt, J., Té, Y., Lu, X., Palm, M., Wang, W., Shan, C., Hu, Q., Qin, M., Tian, Y., and Zheng, B.: The reduction in C_2H_6 from 2015 to 2020 over Hefei, eastern China, points to air quality improvement in China, Atmos. Chem. Phys., 21, 11759-11779, 10.5194/acp-21-11759-2021, 2021a.

Sun, Y., Yin, H., Liu, C., Zhang, L., Cheng, Y., Palm, M., Notholt, J., Lu, X., Vigouroux, C., Zheng, B., Wang, W., Jones, N., Shan, C., Qin, M., Tian, Y., Hu, Q., Meng, F., and Liu, J.: Mapping the drivers of formaldehyde (HCHO) variability from 2015 to 2019 over eastern China: insights from Fourier transform infrared observation and GEOS-Chem model simulation, Atmos. Chem. Phys., 21, 6365-6387, 10.5194/acp-21-6365-2021, 2021b.

Sun, Y., Yin, H., Lu, X., Notholt, J., Palm, M., Liu, C., Tian, Y., and Zheng, B.: The drivers and health risks of unexpected surface ozone enhancements over the Sichuan Basin, China, in 2020, Atmos. Chem. Phys., 21, 18589-18608, 10.5194/acp-21-18589-2021, 2021c.

Sun, Y., Yin, H., Cheng, Y., Zhang, Q., Zheng, B., Notholt, J., Lu, X., Liu, C., Tian, Y., and Liu, J.: Quantifying variability, source, and transport of CO in the urban areas over the Himalayas and Tibetan Plateau, Atmos. Chem. Phys., 21, 9201-9222, 10.5194/acp-21-9201-2021, 2021d.

Sun, Y. W., Liu, C., Palm, M., Vigouroux, C., Notholt, J., Hui, Q. H., Jones, N., Wang, W., Su, W. J., Zhang, W. Q., Shan, C. G., Tian, Y., Xu, X. W., De Maziere, M., Zhou, M. Q., and Liu, J. G.: Ozone

seasonal evolution and photochemical production regime in the polluted troposphere in eastern China derived from high-resolution Fourier transform spectrometry (FTS) observations, Atmos Chem Phys, 18, 14569-14583, 2018.

The NASA Global Modeling and Assimilation Office (GMAO), https://gmao.gsfc.nasa.gov/reanalysis/MERRA-2/, last accessed on 1 April, 2022, 2022.

Vu, T. V., Shi, Z. B., Cheng, J., Zhang, Q., He, K. B., Wang, S. X., and Harrison, R. M.: Assessing the impact of clean air action on air quality trends in Beijing using a machine learning technique, Atmos Chem Phys, 19, 11303-11314, 2019.

Wang, A., and Zeng, X.: Evaluation of multireanalysis products with in situ observations over the Tibetan Plateau, Journal of Geophysical Research: Atmospheres, 117, https://doi.org/10.1029/2011JD016553, 2012.

Xie, Z., Hu, Z., Gu, L., Sun, G., Du, Y., and Yan, X.: Meteorological Forcing Datasets for Blowing Snow Modeling on the Tibetan Plateau: Evaluation and Intercomparison, Journal of Hydrometeorology, 18, 2761-2780, 10.1175/JHM-D-17-0075.1, 2017.

Xu, W., Xu, X., Lin, M., Lin, W., Tarasick, D., Tang, J., Ma, J., and Zheng, X.: Long-term trends of surface ozone and its influencing factors at the Mt Waliguan GAW station, China – Part 2: The roles of anthropogenic emissions and climate variability, Atmos. Chem. Phys., 18, 773-798, 10.5194/acp-18-773-2018, 2018.

Xu, W. Y., Lin, W. L., Xu, X. B., Tang, J., Huang, J. Q., Wu, H., and Zhang, X. C.: Long-term trends of surface ozone and its influencing factors at the Mt Waliguan GAW station, China - Part 1: Overall trends and characteristics, Atmos Chem Phys, 16, 6191-6205, 2016.

Xue, L. K., Wang, T., Zhang, J. M., Zhang, X. C., Deliger, Poon, C. N., Ding, A. J., Zhou, X. H., Wu, W. S., Tang, J., Zhang, Q. Z., and Wang, W. X.: Source of surface ozone and reactive nitrogen speciation at Mount Waliguan in western China: New insights from the 2006 summer study, Journal of Geophysical Research: Atmospheres, 116, https://doi.org/10.1029/2010JD014735, 2011.

Yanai, M. H., Li, C. F., and Song, Z. S.: Seasonal Heating of the Tibetan Plateau and Its Effects on the Evolution of the Asian Summer Monsoon, J Meteorol Soc Jpn, 70, 319-351, 1992.

Yang, R. Q., Zhang, S. J., Li, A., Jiang, G. B., and Jing, C. Y.: Altitudinal and Spatial Signature of Persistent Organic Pollutants in Soil, Lichen, Conifer Needles, and Bark of the Southeast Tibetan Plateau: Implications for Sources and Environmental Cycling, Environmental Science & Technology, 47, 12736-12743, 2013.

Yin, H., Sun, Y., Liu, C., Zhang, L., Lu, X., Wang, W., Shan, C., Hu, Q., Tian, Y., Zhang, C., Su, W., Zhang, H., Palm, M., Notholt, J., and Liu, J.: FTIR time series of stratospheric NO_2 over Hefei, China, and comparisons with OMI and GEOS-Chem model data, Opt Express, 27, A1225-A1240, 10.1364/OE.27.0A1225, 2019a.

Yin, H., Sun, Y., Liu, C., Lu, X., Smale, D., Blumenstock, T., Nagahama, T., Wang, W., Tian, Y., Hu, Q., Shan, C., Zhang, H., and Liu, J.: Ground-based FTIR observation of hydrogen chloride (HCl) over Hefei, China, and comparisons with GEOS-Chem model data and other ground-based FTIR stations data, Opt Express, 28, 8041-8055, 10.1364/OE.384377, 2020.

Yin, H., Liu, C., Hu, Q., Liu, T., Wang, S., Gao, M., Xu, S., Zhang, C., and Su, W.: Opposite impact of emission reduction during the COVID-19 lockdown period on the surface concentrations of $PM_{2.5}$ and O_3 in Wuhan, China, Environmental Pollution, 289, 117899, https://doi.org/10.1016/j.envpol.2021.117899, 2021a.

Yin, H., Lu, X., Sun, Y., Li, K., Gao, M., Zheng, B., and Liu, C.: Unprecedented decline in summertime

surface ozone over eastern China in 2020 comparably attributable to anthropogenic emission reductions and meteorology, Environ Res Lett, 16, 124069, 10.1088/1748-9326/ac3e22, 2021b.

Yin, H., Sun, Y., Notholt, J., Palm, M., and Liu, C.: Spaceborne tropospheric nitrogen dioxide (NO_2) observations from 2005–2020 over the Yangtze River Delta (YRD), China: variabilities, implications, and drivers, Atmos. Chem. Phys., 22, 4167-4185, 10.5194/acp-22-4167-2022, 2022.

Yin, X., Foy, B. D., Wu, K., Feng, C., and Zhang, Q.: Gaseous and particulate pollutants in Lhasa, Tibet during 2013–2017: Spatial variability, temporal variations and implications, Environmental Pollution, 253, 2019b.

Yin, X. F., Kang, S. C., de Foy, B., Cong, Z. Y., Luo, J. L., Zhang, L., Ma, Y. M., Zhang, G. S., Rupakheti, D., and Zhang, Q. G.: Surface ozone at Nam Co in the inland Tibetan Plateau: variation, synthesis comparison and regional representativeness, Atmos Chem Phys, 17, 11293-11311, 2017.

Yin, X. F., de Foy, B., Wu, K. P., Feng, C., Kang, S. C., and Zhang, Q. G.: Gaseous and particulate pollutants in Lhasa, Tibet during 2013-2017: Spatial variability, temporal variations and implications, Environmental Pollution, 253, 68-77, 2019c.

Zhai, S., Jacob, D. J., Wang, X., Shen, L., Li, K., Zhang, Y., Gui, K., Zhao, T., and Liao, H.: Fine particulate matter ($PM_{2.5}$) trends in China, 2013–2018: separating contributions from anthropogenic emissions and meteorology, Atmos. Chem. Phys., 19, 11031-11041, 10.5194/acp-19-11031-2019, 2019.

Zhang, Y. M., Vu, T. V., Sun, J. Y., He, J. J., Shen, X. J., Lin, W. L., Zhang, X. Y., Zhong, J. T., Gao, W. K., Wang, Y. Q., Fu, T. Y., Ma, Y. P., Li, W. J., and Shi, Z. B.: Significant Changes in Chemistry of Fine Particles in Wintertime Beijing from 2007 to 2017: Impact of Clean Air Actions, Environmental Science & Technology, 54, 1344-1352, 2020.

Zhao, S. P., Yu, Y., Yin, D. Y., He, J. J., Liu, N., Qu, J. J., and Xiao, J. H.: Annual and diurnal variations of gaseous and particulate pollutants in 31 provincial capital cities based on in situ air quality monitoring data from China National Environmental Monitoring Center, Environment International, 86, 92-106, 2016.

Zhou, C., Wang, K., and Ma, Q.: Evaluation of Eight Current Reanalyses in Simulating Land Surface Temperature from 1979 to 2003 in China, J Climate, 30, 7379-7398, 10.1175/JCLI-D-16-0903.1, 2017.

Zhu, B., Akimoto, H., Wang, Z., Sudo, K., Tang, J., and Uno, I.: Why does surface ozone peak in summertime at Waliguan?, Geophys Res Lett, 31, 2004.

Zhu, N. L., Fu, J. J., Gao, Y., Ssebugere, P., Wang, Y. W., and Jiang, G. B.: Hexabromocyclododecane in alpine fish from the Tibetan Plateau, China, Environmental Pollution, 181, 7-13, 2013.
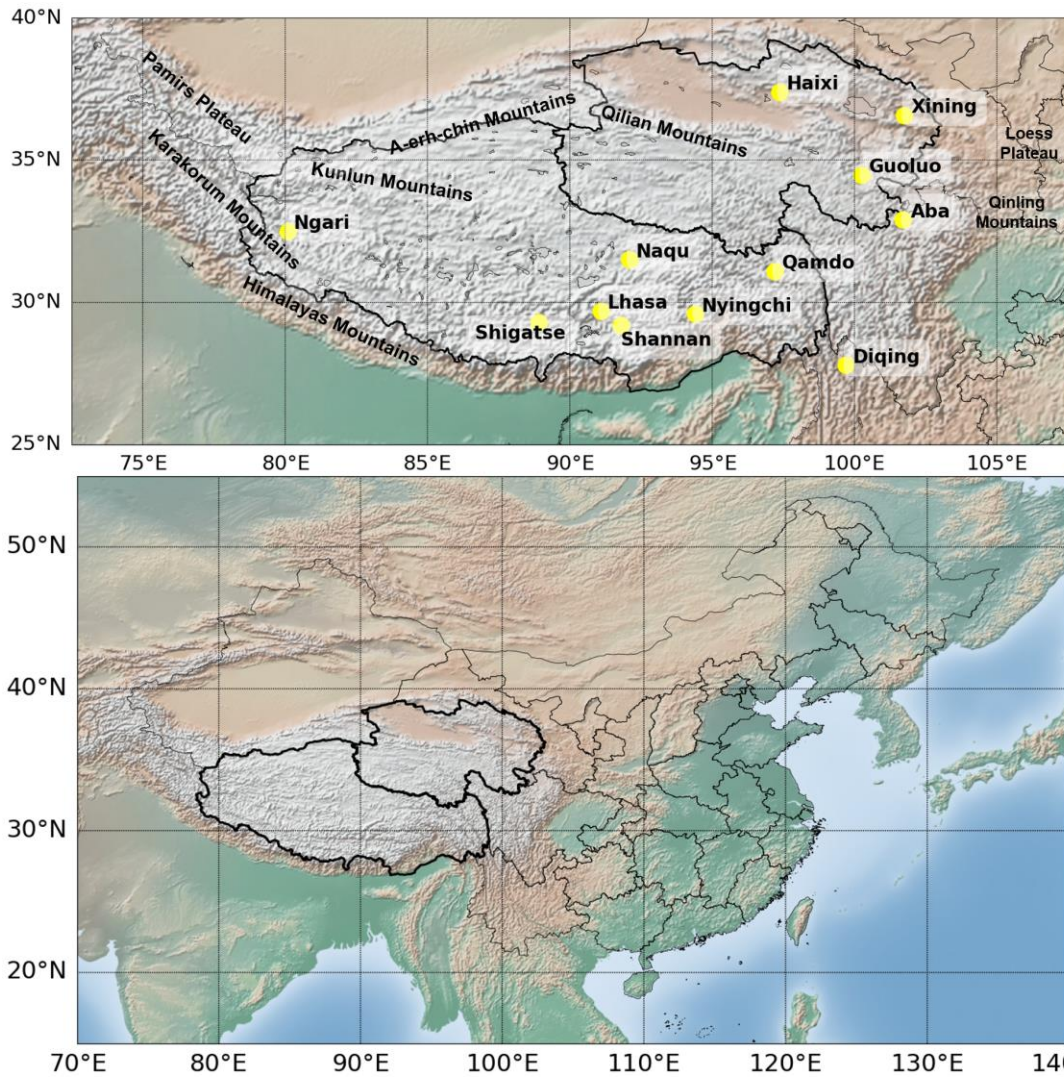
Figure 1. Geolocations of each city over the Qinghai-Tibet Plateau (QTP). The base map of the figure was created using the Basemap package in Python.
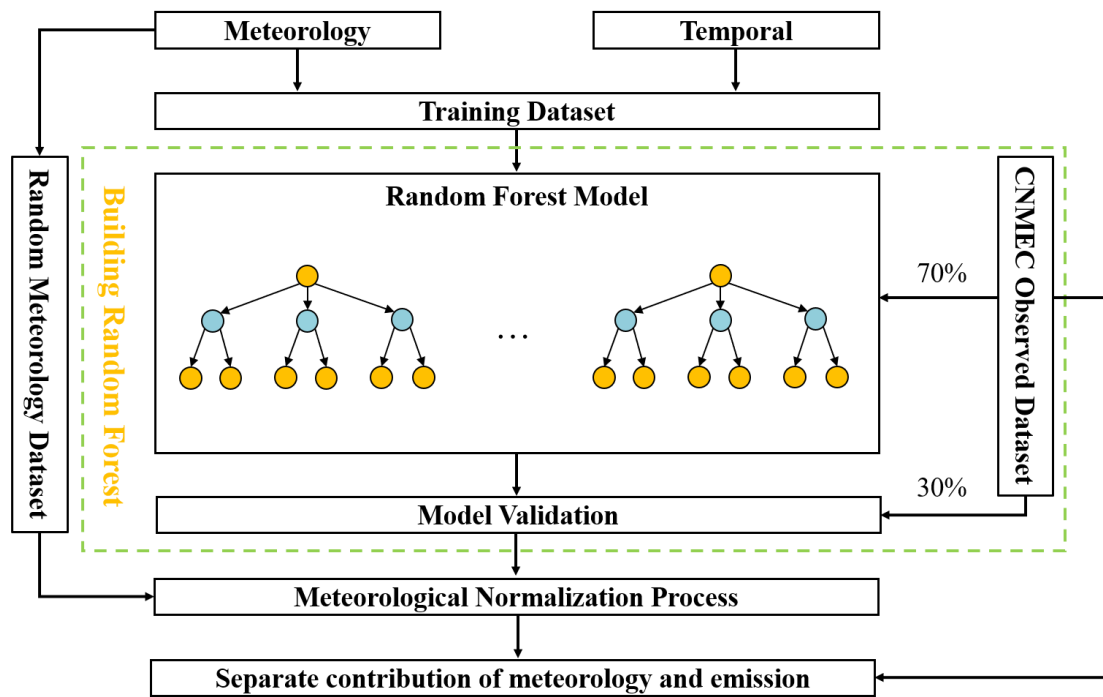
Figure 2. Flowchart for separation of meteorology and anthropologic contributions.
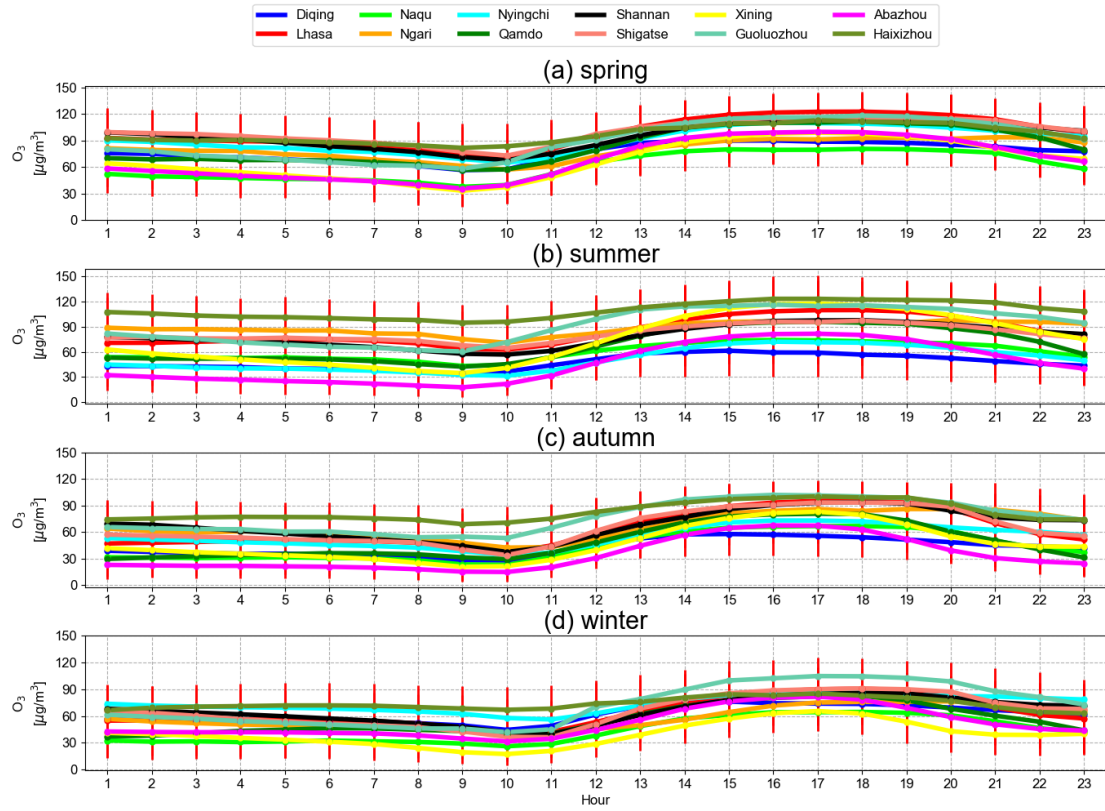
Figure 3. Diurnal cycle of surface ozone (units: μg/m³) in each season and each city over the QTP. The vertical error bar is 1σ standard variation (STD) within that hour.
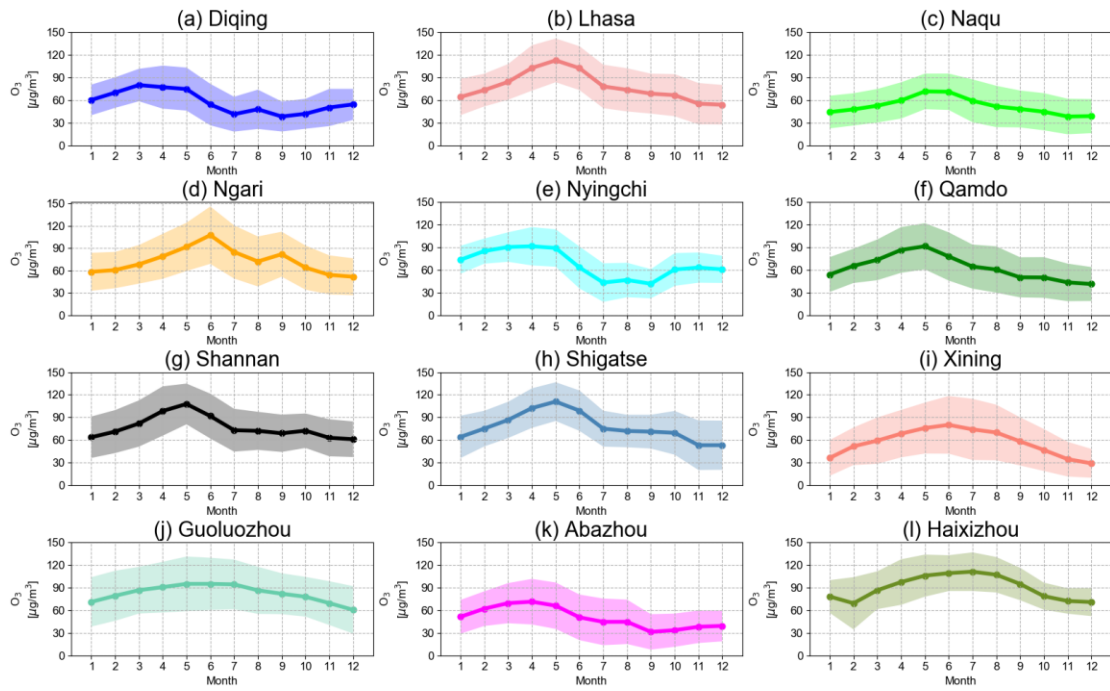
Figure 4. Monthly mean time series of surface ozone (units: μg/m^3) between 2015 and 2020 in each city over the QTP. The vertical error bar is 1σ standard variation (STD) within that month.
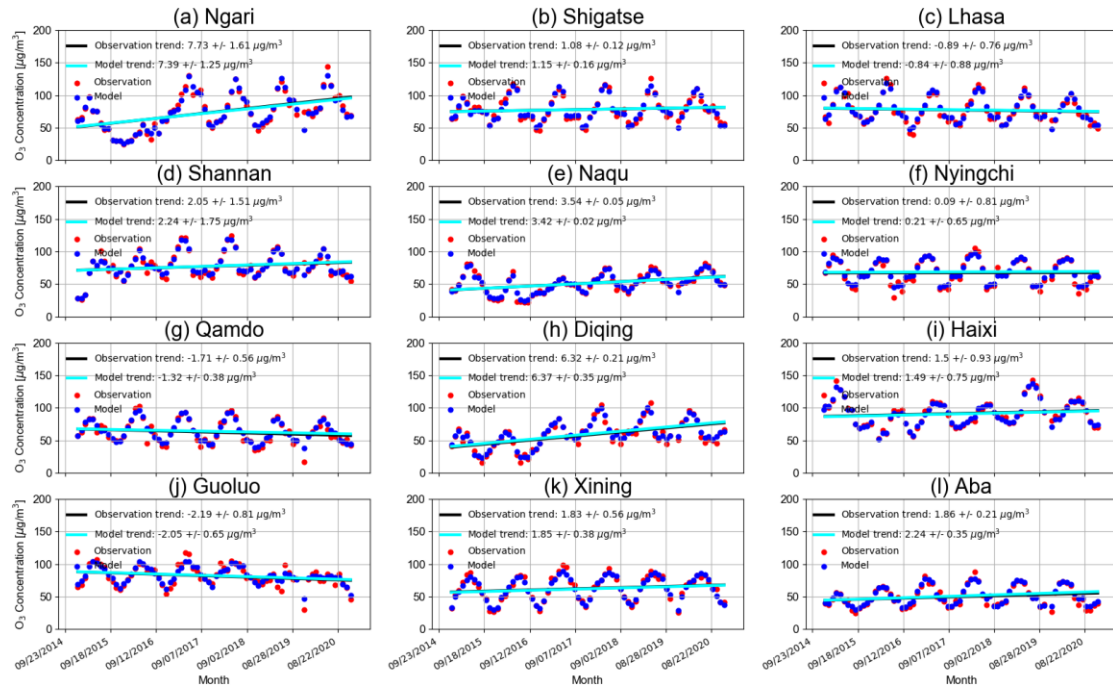
Figure 5. Inter-annual trends of surface ozone levels between 2015 and 2020 in the urban areas over the QTP. Blue dots are the monthly averaged surface ozone measurements. The seasonality and inter-annual variability in each city fitted by using a bootstrap resampling model with a second Fourier series (red dots) plus a linear function (black line) is also shown.
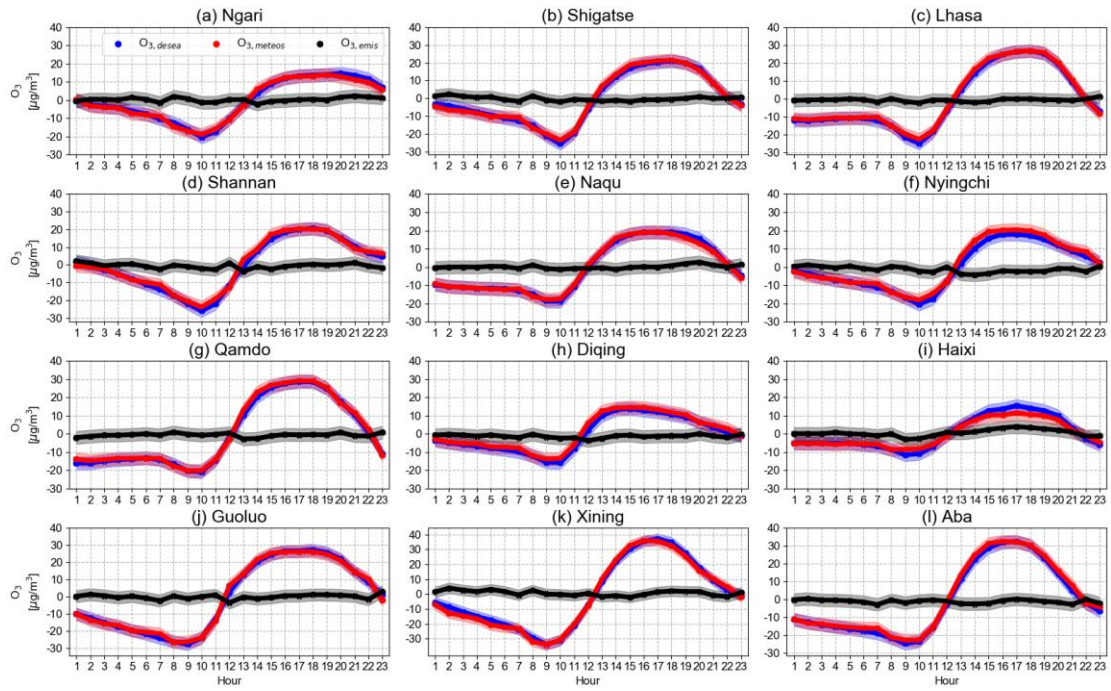
Figure 6. Diurnal cycles of surface ozone anomalies ($O_{3,anomalies}$, blue dots and lines) along with the meteorology-driven portions ($O_{3,meteo}$, red dots and lines) and the anthropogenic-driven portions ($O_{3,emis}$, black dots and lines) in each city over the QTP. Bold curves and the shadows are diurnal cycles and the 1σ standard variations, respectively.
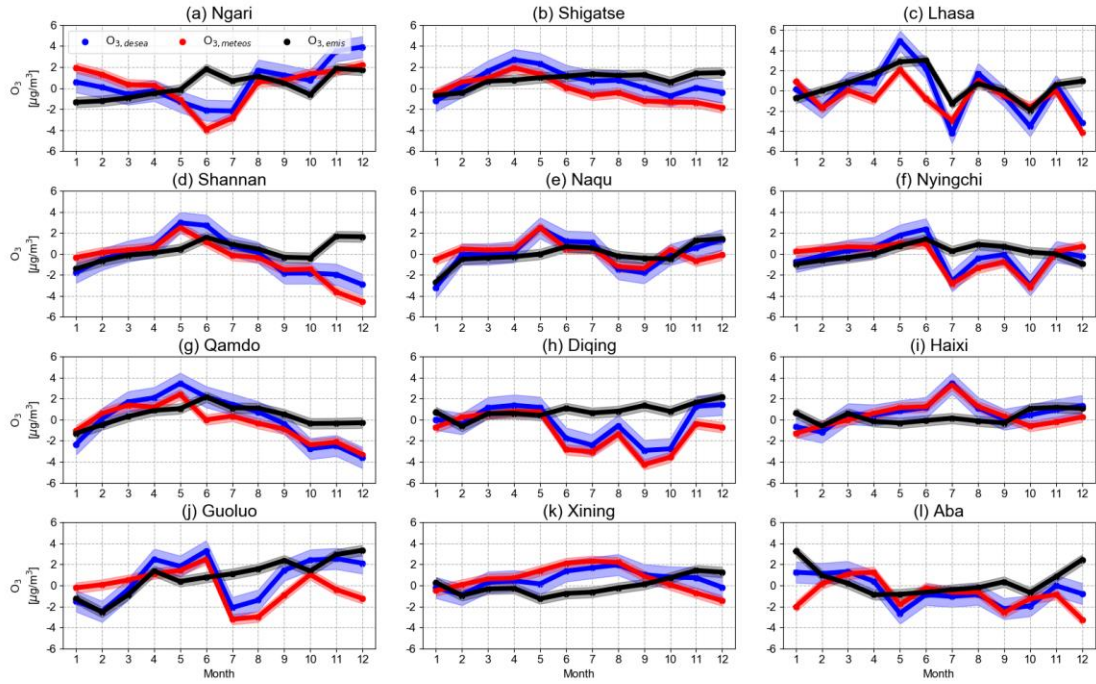
Figure 7. Seasonal cycles of surface ozone anomalies ($O_{3,anomalies}$, blue dots and lines) along with the meteorology-driven portions ($O_{3,meteo}$, red dots and lines) and the anthropogenic-driven portions ($O_{3,emis}$, black dots and lines) in each city over the QTP. Bold curves and the shadows are monthly mean values and the 1σ standard variations, respectively.
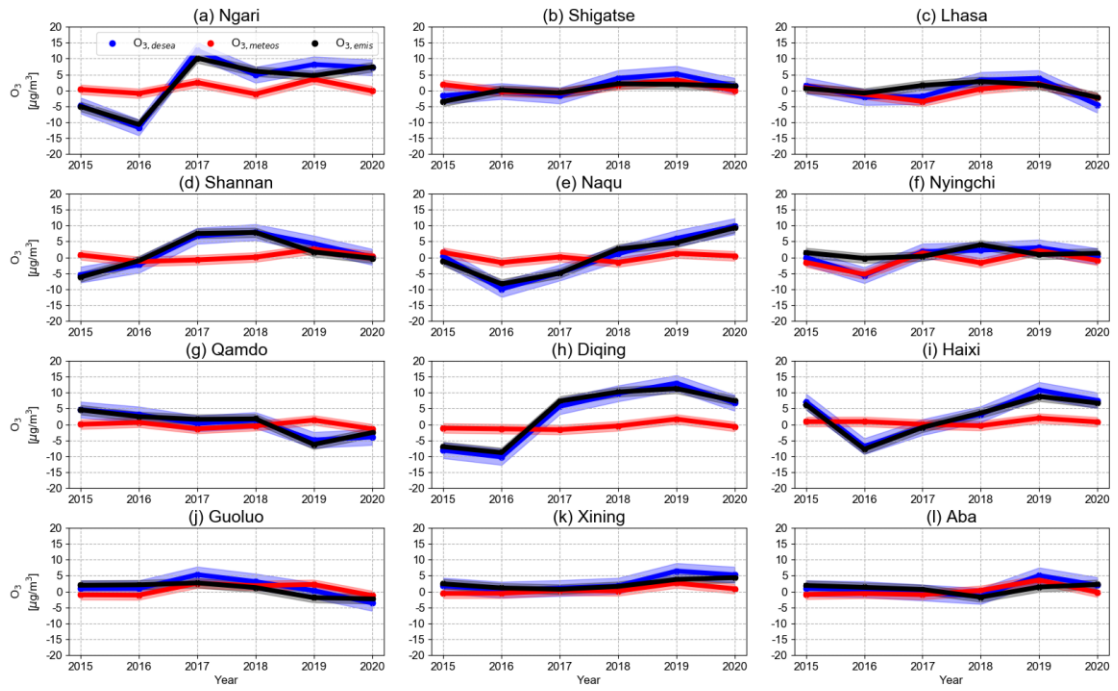
Figure 8. Annual mean surface ozone anomalies ($O_{3,anomalies}$, blue dots and lines) along with meteorology-driven portions ($O_{3,meteo}$, red dots and lines) and anthropogenic-driven portions ($O_{3,emis}$, black dots and lines) in each city over the QTP. Bold curves and the shadows are annual mean values and the 1σ standard variations, respectively.

Table 1. Geolocations of each city over the QTP. Population statistics are available from the 2020 nationwide population census issued by National Bureau of Statistics of China.

Name	Latitude	Longitude	Number of site	Altitude (km)	Population (million)	Area (Thousand km^2)
Ngari	32.5°N	80.1°E	2	4.5	0.12	345.0
Shigatse	29.3°N	88.9°E	3	4.0	0.80	182.0
Lhasa	29.7°N	91.1°E	6	3.7	0.87	31.7
Shannan	29.2°N	91.8°E	2	3.7	0.35	79.3
Naqu	31.5°N	92.1°E	3	4.5	0.50	430.0
Nyingchi	29.6°N	94.4°E	2	3.1	0.23	117.0
Qamdo	31.1°N	97.2°E	3	3.4	0.76	110.0
Diqing	27.8°N	99.7°E	2	3.5	0.39	23.9
Haixi	37.4°N	97.4°E	1	4.8	0.47	325.8
Guoluo	34.5°N	100.3°E	1	4.3	0.21	76.4
Xining	36.6°N	101.7°E	5	2.3	2.47	7.7
Aba	32.9°N	101.7°E	3	3.8	0.82	84.2

Table 2. List of predictive variables fed into the RF model.

Parameters	Description	Unit
Meteorological variables by MERRA-2 dataset		
$T_{surface}$	Surface air temperature	°C
U_{10m}	zonal wind at 10 m height	m/s
V_{10m}	meridional wind at 10 m height	m/s
PBLH	Planetary boundary layer height	m
CLDT	Total cloud area fraction	unitless
PRECTOT	Total Precipitation	kg·m^2/s
OMEGA	Vertical pressure velocity at PBLH	Pa/s
SWGDN	Surface incoming shortwave flux	W/m^2
QV	Specific humidity at 2 m height	kg/kg
TROPT	Tropospheric layer pressure	Pa
Time information		
Year	Year since 2015	/
Month	Month of the year	/
day	Day of the month	/
Hour	Hour of the day	/

1　**Table 3.** Statistical summary of surface ozone concentration (units: μg/m^3) in each city over the
2　QTP from 2015 to 2020.

City	Mean	Standard deviation	Median	The number of nonattainment day					
				2015	2016	2017	2018	2019	2020
Ngari	74.18	34.26	73.50	0	0	8	9	1	13
Shigatse	79.25	31.62	82.00	0	5	0	5	5	2
Lhasa	77.90	32.63	78.67	10	20	2	5	0	0
Shannan	77.55	30.75	78.00	0	2	12	10	2	3
Naqu	52.43	26.27	53.00	0	0	0	0	0	0
Nyingchi	67.30	28.30	68.00	0	0	1	0	0	0
Qamdo	64.23	31.47	62.00	0	2	0	0	0	0
Diqing	57.50	27.64	54.50	0	0	0	0	0	0
Haixi	90.38	28.83	90.00	14	0	0	0	16	2
Guoluo	82.98	33.29	86.00	3	0	3	3	0	0
Xining	63.50	36.02	60.00	0	2	17	6	3	3
Aba	50.67	29.57	47.00	0	0	0	0	0	0

3

Supplement Information

Quantifying the drivers of surface ozone anomalies in the urban areas over the Qinghai-Tibet Plateau

Hao Yin [1, 2,★], Youwen Sun [1, 2,†,★], Justus Notholt [3], Mathias Palm [3], Chunxiang Ye [4], and Cheng Liu [2,5,6,7,†]

[1] *Key Laboratory of Environmental Optics and Technology, Anhui Institute of Optics and Fine Mechanics, HFIPS, Chinese Academy of Sciences, Hefei 230031, China*
[2] *Department of Precision Machinery and Precision Instrumentation, University of Science and Technology of China, Hefei 230026, China*
[3] *University of Bremen, Institute of Environmental Physics, P. O. Box 330440, 28334 Bremen, Germany*
[4] *State Key Laboratory of Environmental Simulation and Pollution Control, College of Environmental Sciences and Engineering, Peking University, Beijing, China*
[5] *Anhui Province Key Laboratory of Polar Environment and Global Change, University of Science and Technology of China, Hefei 230026, China*
[6] *Center for Excellence in Regional Atmospheric Environment, Institute of Urban Environment, Chinese Academy of Sciences, Xiamen 361021, China*
[7] *Key Laboratory of Precision Scientific Instrumentation of Anhui Higher Education Institutes, University of Science and Technology of China, Hefei 230026, China*
[†]Corresponding authors.
[★]These authors contributed equally.
E-mail addresses: Cheng Liu (chliu81@ustc.edu.cn) and Youwen Sun (ywsun@aiofm.ac.cn)

Table S1. Statistical summary of surface ozone concentration (units: μg/m³) in each city over the QTP from 2015 to 2020.

City	Mean	Standard deviation	Median	The number of nonattainment day					
				2015	2016	2017	2018	2019	2020
Ngari	74.18	34.26	73.50	0	0	8	9	1	13
Shigatse	79.25	31.62	82.00	0	5	0	5	5	2
Lhasa	77.90	32.63	78.67	10	20	2	5	0	0
Shannan	77.55	30.75	78.00	0	2	12	10	2	3
Naqu	52.43	26.27	53.00	0	0	0	0	0	0
Nyingchi	67.30	28.30	68.00	0	0	1	0	0	0
Qamdo	64.23	31.47	62.00	0	2	0	0	0	0
Diqing	57.50	27.64	54.50	0	0	0	0	0	0
Haixi	90.38	28.83	90.00	14	0	0	0	16	2
Guoluo	82.98	33.29	86.00	3	0	3	3	0	0
Xining	63.50	36.02	60.00	0	2	17	6	3	3
Aba	50.67	29.57	47.00	0	0	0	0	0	0

Table S1. Diurnal and seasonal cycles (units: $\mu g/m^3$) of surface ozone in each city over the QTP.

City	Diurnal cycle		Seasonal cycle		Interannual trend
	Maximum	Minimum	Maximum	Minimum	($\mu g/m^3 \cdot yr^{-1}$)
Ngari	86.08 ± 22.29 (18:00)	43.07 ± 20.21 (9:00)	107.55 ± 38.43 (June)	51.84 ± 24.72 (December)	7.55 ± 1.61
Shigatse	93.43 ± 14.43 (17:00)	33.92 ± 28.16 (9:00)	110.96 ± 25.60 (May)	53.31 ± 32.82 (September)	0.37 ± 0.12
Lhasa	95.92 ± 15.59 (17:00)	37.14 ± 18.39 (9:00)	112.46 ± 28.92 (May)	53.76 ± 26.14 (December)	-1.62 ± 0.76
Shannan	93.91 ± 14.97 (17:00)	37.60 ± 17.23 (9:00)	107.84 ± 26.93 (April)	61.17 ± 23.54 (December)	1.51 ± 0.36
Naqu	66.86 ± 19.12 (16:00)	22.89 ± 15.55 (9:00)	71.39 ± 23.51 (May)	38.17 ± 22.29 (November)	3.23 ± 0.71
Nyingchi	73.12 ± 16.52 (15:00)	33.79 ± 18.35 (9:00)	91.50 ± 25.33 (April)	41.89 ± 22.29 (September)	0.10 ± 0.81
Qamdo	80.77 ± 15.48 (16:00)	29.31 ± 14.90 (9:00)	91.48 ± 22.29 (May)	41.53 ± 22.29 (December)	-2.43 ± 0.56
Diqing	57.77 ± 21.56 (15:00)	27.94 ± 14.34 (9:00)	79.78 ± 21.48 (March)	38.16 ± 19.83 (September)	5.31 ± 1.28
Haixi	100.36 ± 17.68 (16:00)	68.96 ± 18.27 (8:00)	110.95 ± 25.51 (July)	70.73 ± 16.81 (December)	1.36 ± 0.93
Guoluo	102.08 ± 15.14 (15:00)	53.25 ± 26.27 (8:00)	94.82 ± 34.55 (June)	60.45 ± 31.35 (December)	-2.36 ± 0.81
Xining	82.95 ± 21.15 (16:00)	20.73 ± 15.30 (8:00)	80.23 ± 27.73 (August)	29.21 ± 19.03 (December)	1.83 ± 0.56
Aba	67.50 ± 14.19 (16:00)	14.84 ± 10.77 (8:00)	71.25 ± 26.53 (April)	31.30 ± 22.39 (September)	1.86 ± 0.21

Table S2. The drivers of surface ozone nonattainment events from 2015 to 2020 in each city over the QTP.

City	Number of nonattainment day											
	Anthropogenic-dominated						Meteorology-dominated					
	2015	2016	2017	2018	2019	2020	2015	2016	2017	2018	2019	2020
Ngari	0	0	0	0	0	0	0	0	8	9	0	0
Shigatse	0	0	0	0	0	0	0	5	3	4	5	2
Lhasa	0	0	1	0	0	0	10	20	1	5	0	0
Shannan	0	0	2	0	0	0	0	2	10	10	2	3
Naqu	0	0	0	0	0	0	0	0	0	0	0	0
Nyingchi	0	0	0	0	0	0	0	0	1	0	0	0
Qamdo	0	0	0	0	0	0	0	2	0	0	0	0
Diqing	0	0	0	0	0	0	0	0	0	0	0	0
Haixi	2	0	0	0	1	0	12	0	0	0	15	2
Guoluo	0	0	0	0	0	0	3	0	3	3	0	0
Xining	0	0	0	0	0	0	0	2	17	6	3	3
Aba	0	0	0	0	0	0	0	0	0	0	0	0

Table S3. Inter-annual trends (units: $\mu g \cdot m^{-3} \cdot yr^{-1}$) of surface ozone anomalies, $O_{3,emis}$ and $O_{3,meteos}$ in each city over the QTP fitted by the bootstrap resampling method.

City	Total	$O_{3,emis}$	$O_{3,meteos}$
Ngari	7.55 ± 1.61	7.23 ± 1.25	0.31 ± 0.37
Shigatse	0.37 ± 0.12	0.47 ± 0.16	-0.10 ± 0.16
Lhasa	-1.62 ± 0.76	-1.56 ± 0.88	-0.06 ± 0.38
Shannan	1.51 ± 0.36	1.73 ± 0.37	-0.22 ± 0.33
Naqu	3.23 ± 0.71	3.16 ± 0.79	0.07 ± 0.25
Nyingchi	0.10 ± 0.81	0.22 ± 0.65	-0.12 ± 0.71
Qamdo	-2.43 ± 0.56	-2.00 ± 0.38	-0.43 ± 0.39
Diqing	5.31 ± 1.28	5.40 ± 1.25	-0.09 ± 0.21
Haixi	1.36 ± 0.93	1.35 ± 0.75	0.01 ± 0.15
Guoluo	-2.36 ± 0.81	-2.05 ± 0.65	-0.31 ± 0.16
Xining	1.83 ± 0.56	1.85 ± 0.38	-0.02 ± 0.18
Aba	1.86 ± 0.21	2.25 ± 0.35	-0.39 ± 0.32

Table S4. Correlations of $O_{3, meteo}$ against each meteorological parameter anomalies from 2015 to 2020 over the QTP.

City	Correlations									
	$T_{surface}$	U_{10m}	V_{10m}	PBLH	TCC	Rain	Omega	SWGDN	RH_{2m}	TROPH
Ngari	0.78	0.25	0.40	0.58	-0.08	-0.19	0.31	0.75	-0.40	0.40
Shigatse	0.80	0.27	0.14	0.70	-0.09	-0.23	0.28	0.78	-0.29	0.14
Lhasa	0.83	0.23	-0.03	0.76	-0.12	-0.16	0.36	0.76	-0.20	0.23
Shannan	0.82	0.31	0.15	0.43	-0.18	-0.22	0.27	0.82	-0.26	0.41
Naqu	0.84	0.25	-0.12	0.81	-0.23	-0.31	0.77	0.77	-0.14	0.12
Nyingchi	0.85	-0.35	0.27	0.32	-0.10	-0.25	0.33	0.79	-0.16	0.17
Qamdo	0.81	0.39	-0.16	0.71	-0.15	-0.32	0.14	0.79	-0.18	0.16
Diqing	0.91	0.20	0.43	0.62	-0.06	-0.22	0.32	0.91	-0.21	0.43
Haixi	0.76	0.22	0.21	0.96	-0.21	-0.11	0.50	0.81	-0.40	0.21
Guoluo	0.83	-0.21	-0.12	0.72	-0.36	-0.18	0.56	0.73	-0.39	0.12
Xining	0.87	-0.39	0.27	0.62	-0.28	-0.14	0.26	0.75	-0.19	0.47
Aba	0.91	0.06	-0.15	0.78	-0.12	-0.22	0.35	0.78	-0.11	0.41

Table S5. Correlations of $O_{3, meteo}$ against each meteorological parameter anomalies in diurnal scale from 2015 to 2020 over the QTP.

City	Correlations									
	$T_{surface}$	U_{10m}	V_{10m}	PBLH	TCC	Rain	Omega	SWGDN	RH_{2m}	TROPH
Ngari	0.64	0.20	0.91	0.62	-0.16	-0.22	0.71	0.55	-0.21	0.43
Shigatse	0.72	0.22	0.73	0.76	-0.31	-0.31	0.23	0.53	-0.48	0.23
Lhasa	0.76	0.25	-0.82	0.81	-0.32	-0.51	0.57	0.64	-0.43	0.12
Shannan	0.73	0.35	0.38	0.58	-0.18	-0.09	0.53	0.60	-0.40	0.39
Naqu	0.74	-0.15	0.68	0.72	-0.10	-0.34	0.69	0.63	-0.34	0.37
Nyingchi	0.72	0.49	-0.79	0.71	-0.25	-0.32	0.64	0.64	-0.23	0.16
Qamdo	0.77	0.31	0.75	0.42	-0.22	-0.52	0.27	0.75	-0.10	0.32
Diqing	0.80	0.70	0.78	0.70	-0.19	-0.03	0.73	0.69	-0.29	0.14
Haixi	0.73	-0.60	0.27	0.63	-0.15	-0.56	0.76	0.89	-0.15	0.51
Guoluo	0.75	-0.21	-0.93	0.72	-0.16	-0.38	0.36	0.70	-0.49	0.12
Xining	0.89	-0.06	-0.96	0.78	-0.12	-0.21	0.35	0.91	-0.41	0.40
Aba	0.95	0.52	-0.33	0.96	-0.21	-0.32	0.80	0.72	-0.40	0.20

Table S6. Correlations of $O_{3, meteo}$ against each meteorological parameter anomalies in seasonal scale from 2015 to 2020 over the QTP.

City	Correlations									
	$T_{surface}$	U_{10m}	V_{10m}	PBLH	TCC	Rain	Omega	SWGDN	RH_{2m}	TROPH
Ngari	0.80	0.20	-0.05	0.68	-0.20	-0.21	0.64	0.57	-0.50	0.40
Shigatse	0.81	-0.34	0.21	0.77	-0.25	-0.26	0.58	0.92	-0.19	0.27
Lhasa	0.83	-0.45	-0.07	0.65	-0.22	-0.31	0.25	0.88	-0.32	0.38
Shannan	0.86	-0.20	-0.64	0.69	-0.33	-0.45	0.34	0.95	-0.57	0.62
Naqu	0.87	0.36	0.16	0.60	-0.29	-0.16	0.33	0.63	-0.38	0.61
Nyingchi	0.83	-0.09	-0.36	0.67	-0.21	-0.34	0.51	0.73	-0.11	0.26
Qamdo	0.83	-0.21	0.18	0.75	-0.31	-0.27	0.57	0.90	-0.15	0.28
Diqing	0.92	-0.14	0.23	0.70	-0.33	-0.06	0.58	0.84	-0.12	0.16
Haixi	0.87	-0.40	-0.76	0.90	-0.34	-0.28	0.69	0.64	-0.32	0.67
Guoluo	0.96	-0.21	-0.89	0.79	-0.21	-0.36	0.79	0.92	-0.64	0.46
Xining	0.83	0.27	-0.73	0.71	-0.36	-0.28	0.37	0.96	-0.35	0.59
Aba	0.92	-0.25	-0.66	0.95	-0.27	-0.32	0.87	0.72	-0.32	0.50

Table S7. Correlations of $O_{3, meteo}$ against each meteorological parameter anomalies in multi-year scale from 2015 to 2020 over the QTP.

City	Correlations									
	$T_{surface}$	U_{10m}	V_{10m}	PBLH	TCC	Rain	Omega	SWGDN	RH_{2m}	TROPH
Ngari	0.79	0.51	0.75	0.66	-0.29	-0.34	0.77	0.64	-0.43	0.39
Shigatse	0.82	-0.11	-0.11	0.76	-0.19	-0.18	0.53	0.71	-0.18	0.16
Lhasa	0.86	-0.30	-0.51	0.86	-0.37	-0.29	0.38	0.65	-0.53	0.33
Shannan	0.91	0.16	-0.16	0.81	-0.15	-0.11	0.29	0.75	-0.28	0.53
Naqu	0.82	-0.82	0.80	0.86	-0.29	-0.16	0.23	0.85	-0.46	0.56
Nyingchi	0.91	0.28	-0.97	0.98	-0.39	-0.17	0.66	0.84	-0.53	0.73
Qamdo	0.93	0.88	-0.88	0.85	-0.18	-0.25	0.72	0.86	-0.55	0.61
Diqing	0.90	-0.85	-0.90	0.95	-0.38	-0.23	0.61	0.92	-0.35	0.80
Haixi	0.84	-0.83	-0.51	0.81	-0.57	-0.29	0.63	0.78	-0.50	0.85
Guoluo	0.88	-0.79	-0.85	0.84	-0.36	-0.30	0.53	0.87	-0.34	0.52
Xining	0.80	-0.55	0.40	0.84	-0.20	-0.28	0.32	0.78	-0.39	0.64
Aba	0.92	-0.19	0.53	0.92	-0.10	-0.34	0.76	0.87	-0.40	0.49

Table S8. The correlations between each meteorological variable and ozone anomalies in each city over the QTP region during ozone nonattainment events.

City	Correlations									
	$T_{surface}$	U_{10m}	V_{10m}	PBLH	TCC	Rain	Omega	SWGDN	RH_{2m}	TROPH
Ngari	0.57	-0.45	-0.13	0.09	0.35	0.38	0.32	-0.25	-0.02	0.16
Shigatse	0.69	0.38	-0.02	0.29	-0.13	-0.37	0.31	-0.37	-0.36	0.23
Lhasa	0.51	0.35	-0.12	0.34	-0.15	-0.39	0.35	0.02	-0.36	0.18
Shannan	0.67	-0.22	-0.25	0.02	0.22	0.14	0.25	-0.04	-0.11	0.32
Naqu	NA[1]	NA	NA	NA	NA	NA	NA	NA	NA	NA
Nyingchi	NA	NA	NA	NA	NA	NA	NA	NA	NA	NA
Qamdo	NA	NA	NA	NA	NA	NA	NA	NA	NA	NA
Diqing	NA	NA	NA	NA	NA	NA	NA	NA	NA	NA
Haixi	0.83	0.28	-0.08	0.40	0.10	0.23	0.22	-0.77	-0.38	0.30
Guoluo	0.52	-0.76	-0.34	0.15	0.39	-0.12	0.69	0.45	-0.34	0.33
Xining	0.69	-0.20	-0.37	0.34	0.35	0.45	0.36	0.08	-0.20	0.31
Aba	NA	NA	NA	NA	NA	NA	NA	NA	NA	NA

[1] In these cities, there is no ozone nonattainment events during 2015 to 2020, expected Qamdo. In Qamdo, the ozone nonattainment events are only in 2 days. Therefore, we cannot calculate the correlations between each meteorological variable and ozone anomalies in these cities.

Table S9. The anthropogenic emissions of monthly total NO_x from 2015 to 2020 at each city over the QTP. (Units: t)

City	1	2	3	4	5	6	7	8	9	10	11	12
Ngari	0.20	0.20	0.22	0.22	0.22	0.24	0.22	0.23	0.22	0.22	0.21	0.20
Shigatse	5.54	5.56	5.85	5.95	6.03	6.26	5.98	6.04	5.97	5.88	5.79	5.54
Lhasa	68.51	69.61	82.56	87.52	91.02	101.27	89.05	91.53	88.52	84.42	79.61	68.67
Shannan	8.09	8.23	9.89	10.52	10.96	12.28	10.71	11.03	10.64	10.12	9.52	8.11
Naqu	1.99	2.00	2.21	2.28	2.34	2.51	2.30	2.34	2.29	2.23	2.17	1.99
Nyingchi	1.32	1.35	1.70	1.83	1.93	2.21	1.87	1.94	1.86	1.75	1.62	1.32
Qamdo	5.53	5.54	5.75	5.82	5.87	6.04	5.84	5.88	5.83	5.77	5.70	5.53
Diqing	8.13	6.80	8.37	8.32	7.99	8.35	7.80	8.01	8.74	8.30	9.28	9.66
Haixi	38.72	31.92	34.47	36.21	30.08	30.65	29.77	27.37	29.65	37.99	36.50	35.51
Guoluo	5.39	4.63	5.39	6.43	5.77	5.91	6.23	6.93	6.25	6.56	7.60	7.64
Xining	11.16	10.72	11.80	12.70	12.42	12.68	12.66	12.88	13.51	13.50	13.75	13.20
Aba	0.73	0.65	0.63	0.62	0.62	0.62	0.61	0.61	0.61	0.61	0.62	0.66

Table S10. The anthropogenic emissions of monthly total VOCs from 2015 to 2020 at each city over the QTP. (Units: t)

City	1	2	3	4	5	6	7	8	9	10	11	12
Ngari	0.11	0.64	0.80	1.06	1.01	1.17	0.95	1.10	1.20	0.72	2.34	2.14
Shigatse	1.59	1.69	1.77	1.82	1.80	1.91	1.80	1.84	1.82	1.73	2.10	2.00
Lhasa	21.51	50.83	62.66	78.25	75.99	87.45	72.76	81.32	85.73	58.93	146.36	132.92
Shannan	2.52	9.46	11.93	15.41	14.75	17.19	13.99	15.97	17.14	10.89	31.98	29.05
Naqu	0.71	2.57	3.17	4.06	3.85	4.46	3.65	4.17	4.50	2.85	8.61	7.87
Nyingchi	0.40	0.42	0.50	0.54	0.55	0.63	0.54	0.56	0.54	0.51	0.54	0.46
Qamdo	1.56	1.62	1.68	1.74	1.73	1.82	1.75	1.77	1.75	1.69	1.86	1.80
Diqing	14.16	11.67	14.62	13.29	11.14	11.52	10.66	11.43	13.19	11.68	13.11	14.76
Haixi	20.92	18.03	19.89	23.61	20.91	21.78	23.23	25.17	22.23	23.54	27.21	27.30
Guoluo	10.08	8.64	9.54	11.59	10.27	10.73	11.51	12.54	10.84	11.45	13.14	13.29
Xining	14.64	13.50	13.57	13.00	11.60	11.92	12.29	12.77	12.29	13.20	16.58	16.50
Aba	1.77	1.20	1.07	1.02	1.06	1.10	1.05	1.04	1.07	1.06	1.10	1.39

Table S11. The anthropogenic emissions of annual total NO_x from 2015 to 2020 at each city over the QTP. (Units: t)

City	2015	2016	2017
Ngari	0.25	0.20	0.22
Shigatse	5.82	5.96	5.92
Lhasa	82.14	83.70	84.74
Shannan	9.79	10.06	10.18
Naqu	2.28	2.18	2.23
Nyingchi	1.67	1.74	1.76
Qamdo	5.85	5.73	5.69
Diqing	8.69	8.08	8.16
Haixi	37.55	30.73	31.54
Guoluo	6.02	6.10	6.26
Xining	13.17	12.41	12.16
Aba	0.66	0.62	0.61

Table S12. The anthropogenic emissions of monthly total VOCs from 2015 to 2020 at each city over the QTP. (Units: t)

City	2015	2016	2017
Ngari	1.16	1.11	1.18
Shigatse	1.68	1.82	1.79
Lhasa	77.16	79.70	81.82
Shannan	15.11	15.91	16.55
Naqu	4.51	4.22	4.38
Nyingchi	0.54	0.52	0.49
Qamdo	1.90	1.70	1.59
Diqing	12.66	12.40	12.75
Haixi	21.96	22.63	23.87
Guoluo	10.71	10.99	11.72
Xining	13.71	13.47	13.29
Aba	1.22	1.15	1.11

Table S13. The correlations between the monthly averaged anthropogenic contributions and NO_x and VOCs emissions by MEIC inventory.

City	$R_{NO_x-month}$	$R_{VOC-month}$	R_{NO_x-year}	$R_{VOC-year}$
Ngari	0.74	0.62	0.15	0.88
Shigatse	0.58	0.61	0.56	0.62
Lhasa	0.43	0.33	0.28	0.34
Shannan	0.35	0.65	0.94	0.98
Naqu	0.56	0.66	0.78	0.82
Nyingchi	0.65	0.61	-0.84	0.54
Qamdo	0.75	0.35	0.82	0.83
Diqing	0.66	0.55	-0.29	0.77
Haixizhou	0.81	0.39	0.92	-0.36
Guoluozhou	0.74	0.71	0.93	0.92
Xining	0.55	0.83	0.91	0.90
Abazhou	0.77	0.67	0.87	0.89
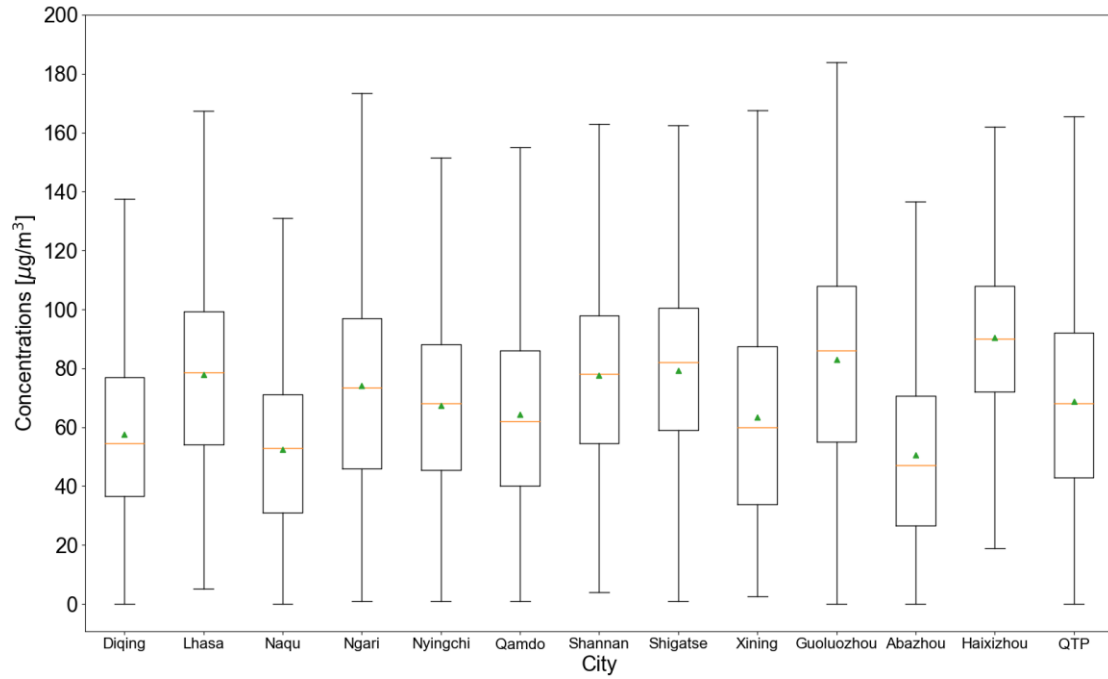
Figure S1. Boxplot of surface ozone (units: $\mu g/m^3$) from 2015 to 2020 in each city over the QTP. Lower and upper box boundaries represent 25th and 75th percentiles, respectively; line and triangle inside box represent median and mean, respectively; lower and upper error lines represent 1.5*IQR (interquartile range) below the third quartile and above the first quartile, respectively.
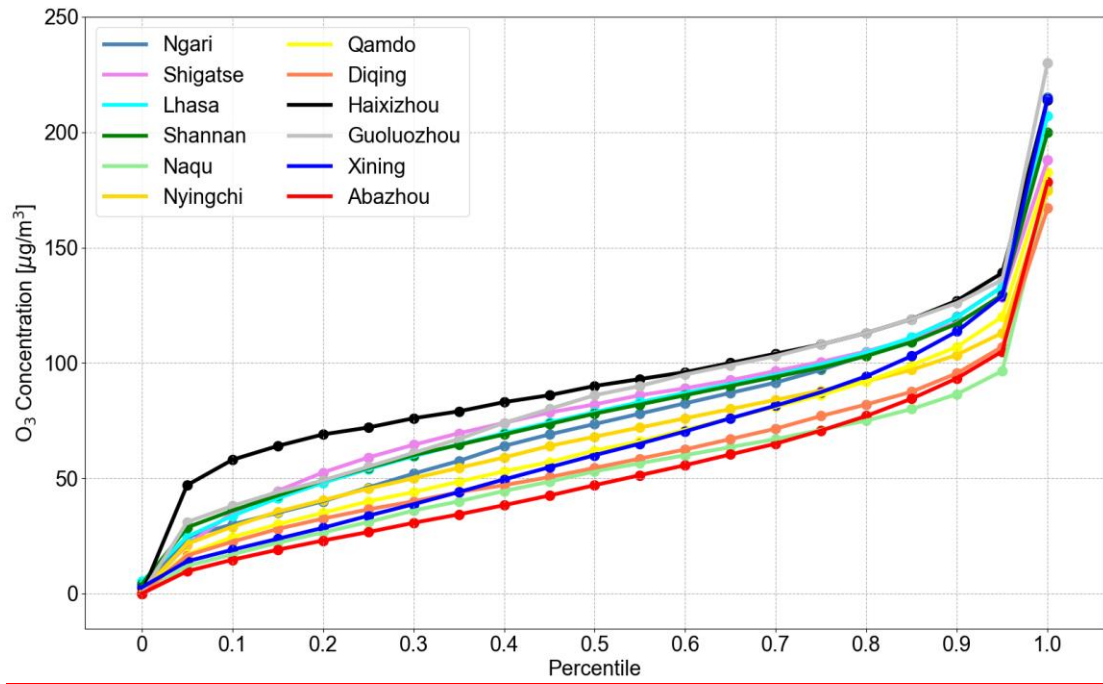
Figure S2. The percentile variation of surface ozone concentration (units: μg/m^3) in each city over the QTP from 2015 to 2020.
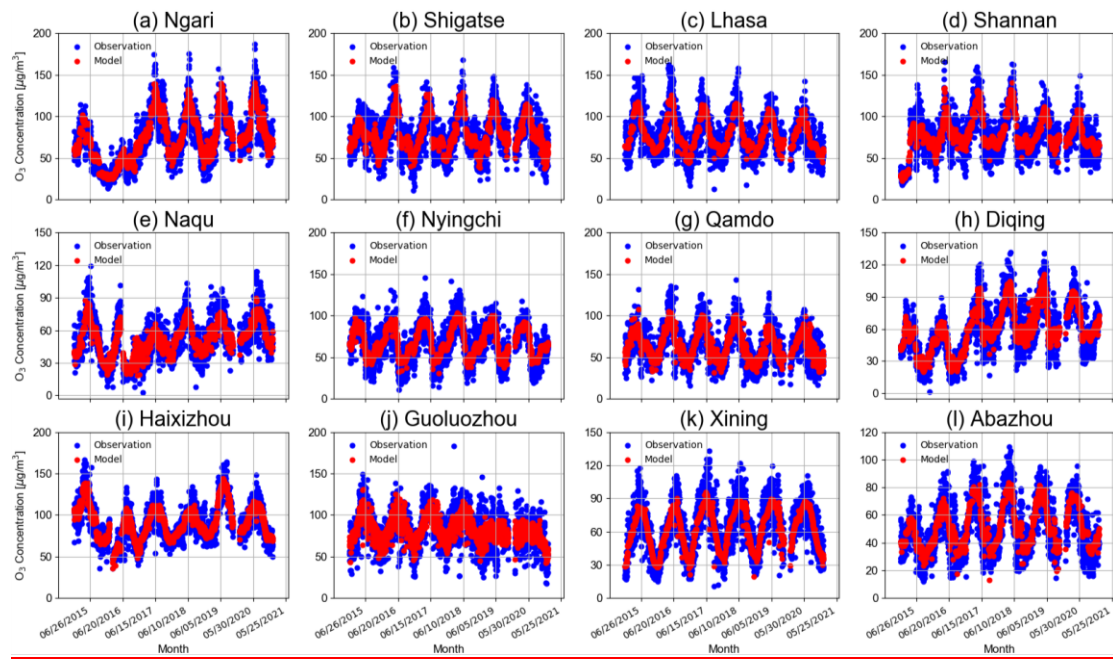
Figure S3. The time series of surface ozone observations and meteorological normalization data in each city over the QTP region from 2015 to 2020.
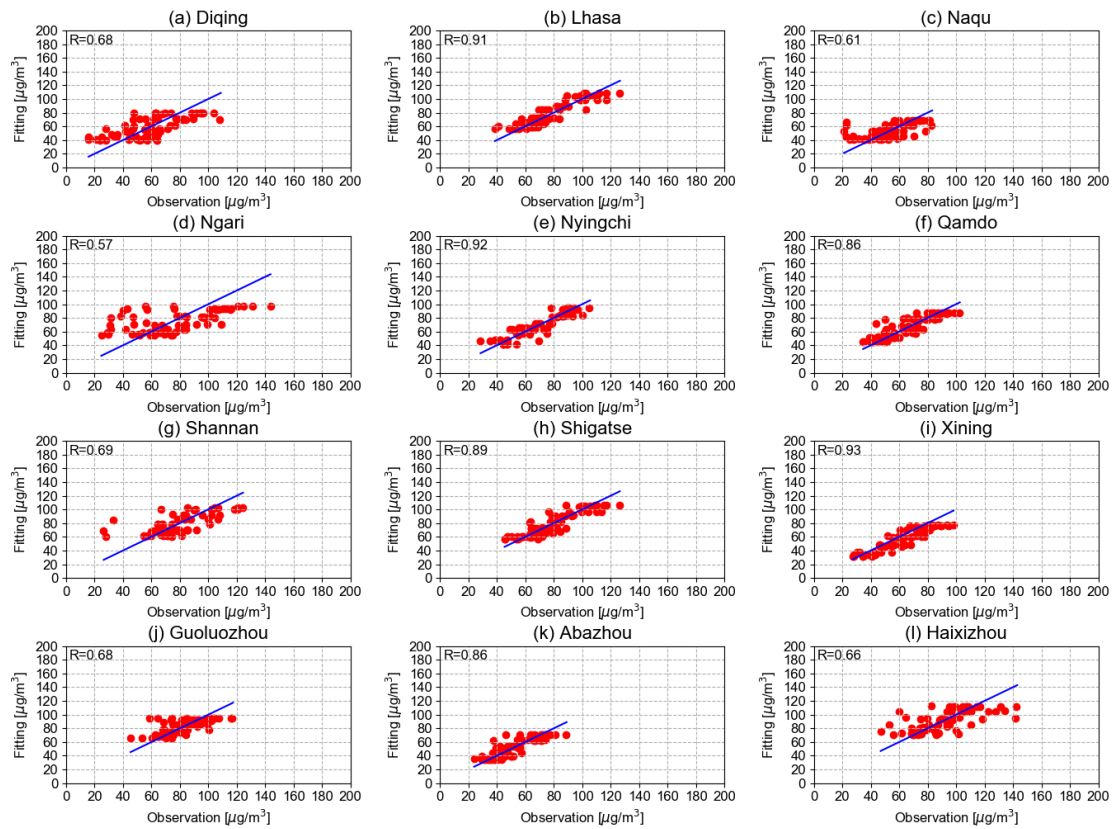
Figure S4. The comparisons of measured and fitted surface ozone concentrations in each city over the QTP region.
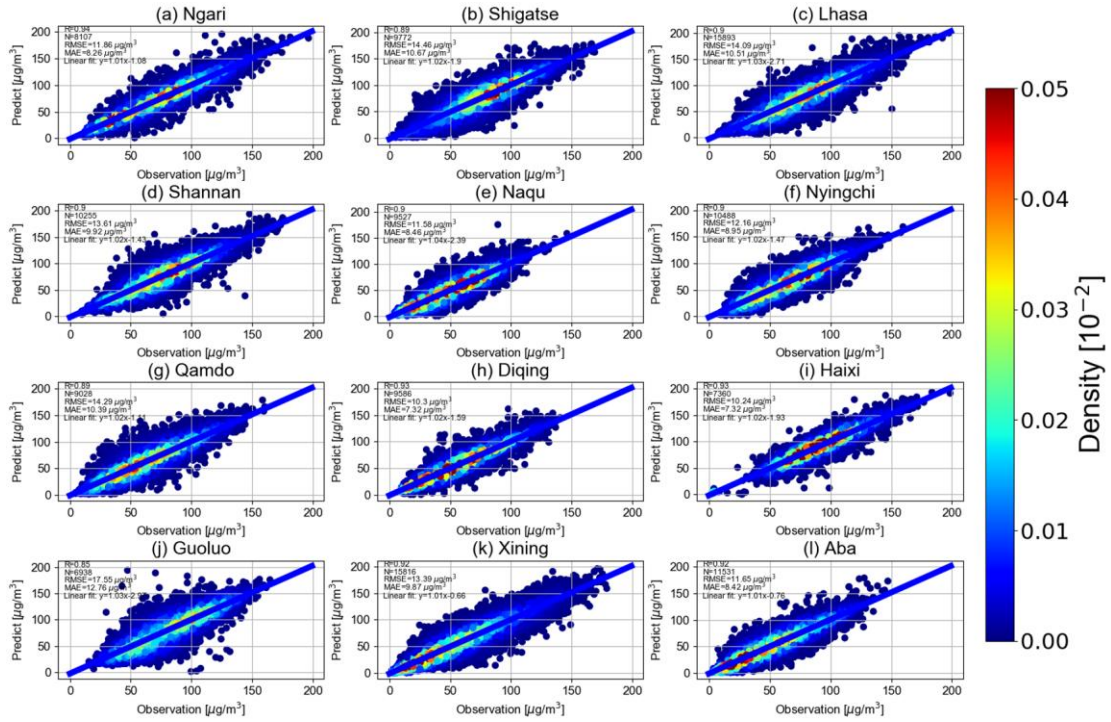
Figure S5. Performance of the RF model in predicting hourly surface ozone levels in each city over the QTP. The model was constructed with 70% training data and validated with the remaining 30% testing data. The plots show the comparisons between the model predictions and measurements for the 30% testing data in each city over the QTP. The blue lines are linear fitted curves of the respective scatter points. The colors represent probability distribution densities.
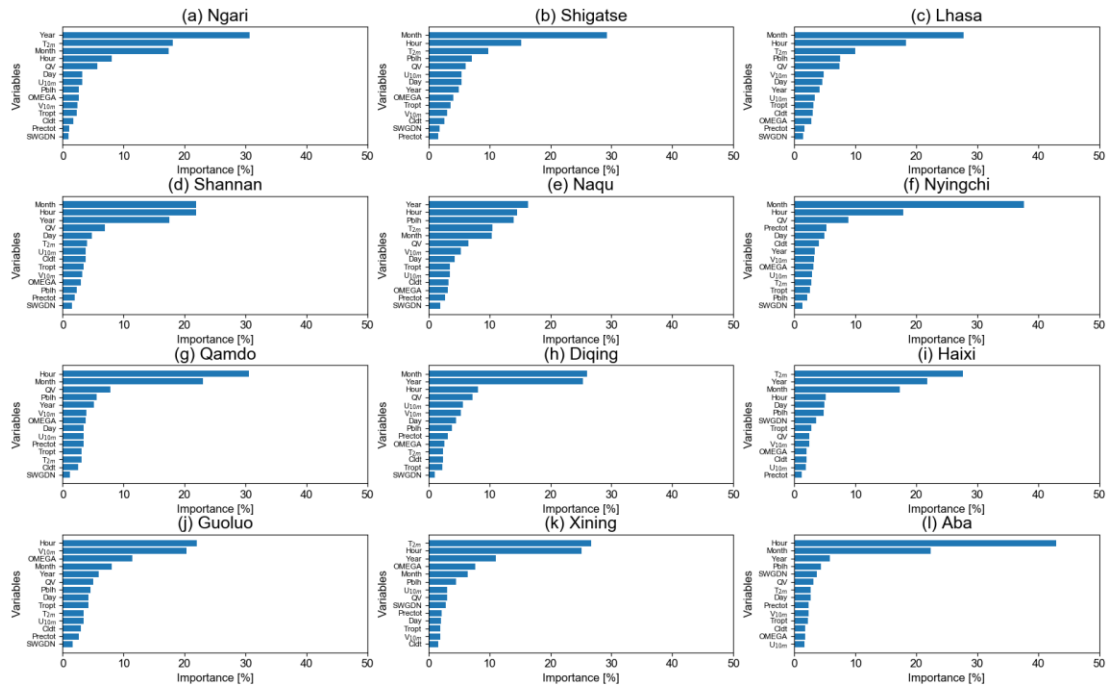
Figure S6. Importance scores (%) of each predictive variable, including Temperature (T_{2m}), Winds (U_{10m}, V_{10m}), Planetary boundary layer height (PBLH), Total cloud are fraction (CLDT), Rainfall (PRECTOT), Vertical pressure velocity (OMEGA), Surface incoming shortwave flux (SWGDN), Specific humidity (QV), Tropospheric layer Pressure (TROPT) and time information (Year, Month, Day and Hour), considered for predicting surface ozone levels in each city over the QTP using the RF model.